

# Efficient Multidimensional Functional Data Analysis Using Marginal Product Basis Systems

William Consagra

Department of Biostatistics and Computational Biology  
University of Rochester, Rochester, New York, U.S.A.

Arun Venkataraman

Department of Physics and Astronomy  
University of Rochester, Rochester, New York, U.S.A.

Xing Qiu\*

Department of Biostatistics and Computational Biology  
University of Rochester, Rochester, New York, U.S.A.

August 2, 2021

---

\*Correspondence should be sent to XQ (E-mail: xing\_qiu@urmc.rochester.edu). This work is supported in part by the University of Rochester CTSA award number UL1 TR002001 from the National Center for Advancing Translational Sciences of the National Institutes of Health.

## Abstract

Modern datasets, from areas such as neuroimaging and geostatistics, often come in the form of a random sample of tensor-valued data which can be understood as noisy observations of an underlying smooth multidimensional random function. Many of the traditional techniques from functional data analysis are plagued by the curse of dimensionality and quickly become intractable as the dimension of the domain increases. In this paper, we propose a framework for learning multidimensional continuous representations from a random sample of tensors that is immune to several manifestations of the curse. These representations are defined to be multiplicatively separable and adapted to the data according to an  $L^2$  optimality criteria, analogous to a multidimensional functional principal components analysis. We show that the resulting estimation problem can be solved efficiently by the tensor decomposition of a carefully defined reduction transformation of the observed data. The incorporation of both regularization and dimensionality reduction is discussed. The advantages of the proposed method over competing methods are demonstrated in a simulation study. We conclude with a real data application in neuroimaging.

*Keywords:* Multidimensional functional data analysis; marginal product basis; basis representation; tensor decomposition; universal approximation; functional principal component analysis

# 1 Introduction

Functional data analysis (FDA) is a subfield of statistics concerned with the analysis of collections of smooth functions. Most of the foundational work in FDA considers the 1-dimensional case, i.e. when the function domain of definition is an interval on  $\mathbb{R}^1$ , usually understood to represent time (Ramsay, 2005; Hsing and Eubank, 2015). Although many modern datasets from fields such as neuroimaging, chemometrics, climate science, and astronomy can be modeled as random functions/fields defined on multidimensional and/or non-Euclidean domains, there has been a relative lack of attention to extending FDA techniques to these cases. This can be largely attributed to the fact that many of the traditionally used approaches in FDA have a tendency to become computationally intractable as the dimension of the problem increases, a manifestation of the so-called *curse of dimensionality*.

For most FDA applications, the analyst only has access to discrete and noisy observations of the underlying random function. Therefore, a common approach to analysis is to perform the initial step of estimating a smooth function from each subject's discretely observed data (Zhang and Chen, 2007), referred to here as *functional representation*. A host of downstream analyses, such as functional principal components analysis (FPCA), regression, and ordinary/partial differential equation modeling, are then performed on these reconstructed smooth functions. In 1-dimension, functional representation is typically accomplished by nonparametric estimation through either local polynomial/kernel regression or by expansion over some appropriately defined basis system, e.g. various splines. Unfortunately, these approaches suffer from the curse of dimensionality when extended to multidimensional cases. The number of observations required to obtain a desired mean-squared error (Stone, 1980) and/or the number of model parameters (e.g. the number of basis functions for a tensor product basis) grow exponentially in  $D$ , the dimension of the domain (Wasserman, 2010). To avoid these issues, a common tactic is to impose some structural assumptions on the nature of the underlying functions, leading to the development of the so-called semiparametric regression models such as additive and single index models (Ruppert et al., 2006). Although the semi-structured nature permits efficient estimation, these frameworks are often overly restrictive for real world data exhibiting complex dependence patterns.

In what follows, we propose a framework for multidimensional FDA based on learning the optimal *marginal product basis* (MPB) for representing realizations of a  $D$ -dimensional random field. Heuristically, a function is referred to as a marginal product function (MPF) if it is multiplicatively separable over some product domain, see Definition 2.1; and an MPB is simply a collection of linearly independent MPFs. Crucially, the number of parameters needed to estimate the MPB is not exponential in  $D$ , yet it still retains much of the flexibility of the nonparametric models, which is epitomized in a universal approximation property (see Section 2.1). For these reasons, this structure has been used to facilitate efficient procedures for a variety of related tasks in multidimensional function approximation from scattered data (Beylkin et al., 2009; Chevreuril et al., 2015), or data observed on a grid (Grasedyck et al., 2013; Gorodetsky et al., 2015). It has also been employed for the canonical nonparametric regression task, i.e. when the function is observed with *i.i.d.* error (Suzuki et al., 2016; Kargas and Sidiropoulos, 2021), for estimating the fixed effects in functional ANOVA (Huang et al., 2009) and in the context of reduced basis methods and dictionary learning (Nouy, 2017).

Unfortunately, there has been a relative lack of attention to this structure in the context of modeling random functions. This is likely because of the well known optimality of basis systems constructed from the eigenfunctions of the covariance operator, and therefore much of the past work on random function representation has been focused on their estimation (Silverman, 1996; Yao et al., 2005). Estimating the eigenfunctions, i.e. performing FPCA, for a  $D$ -dimensional random function is typically accomplished through estimation of the  $2D$ -dimensional covariance function. Some techniques have recently been proposed (Chen and Jiang, 2017; Li et al., 2019; Wang et al., 2020), although this approach can become untenable as  $D$  becomes even moderately large. In this work, we show that by using the MPB structure, we can estimate a data-adaptive functional space for efficient representation of functional data while avoiding the “dimension doubling” involved in the estimation of the covariance function. Furthermore, we provide a convergence rate for the expected approximation error of the optimal rank- $K$  MPB in the general case.

Our method is related to the work in Allen (2013), who propose an algorithm for smoothing general functions of  $D$ -dimensional domains using a penalized tensor decomposition

algorithm, coined FCP-TPA. The FCP-TPA algorithm constructs an approximate solution to the multidimensional analogue of the optimization problem proposed for smoothing  $D = 2$  dimensional functional data in Huang et al. (2009) and allows for the incorporation of penalties with respect to known smoothness structure, e.g. second order finite differences. Along with the follow up work in Allen and Weylandt (2019), they implicitly assume a joint MPF structure for functional data observed on a grid and propose methods to estimate the basis function evaluations at the grid points. As a result, the estimated factors are of the *same dimensionality* as the observed discrete data tensor. One of the key contributions of our work is that we show that the optimal rank- $K$  MPB can be obtained from the canonical polyadic decomposition (CPD) of a tensor  $\widehat{\mathcal{G}}$  that is computed from the observed data via a *reduction transformation*. This permits user-control of the dimension of the resulting optimization problem, which can result in huge computational gains when the sampling domain is large. Furthermore, FCP-TPA requires a *post hoc* projection to obtain a continuous representation of the data, whereas our method provides a fully functional treatment of the problem. The advantages of working directly with continuous representations are plentiful but may be encompassed by the idea that complex operations on functions can be constructed explicitly from simpler ones. When working directly with the discrete data, such operations can be potentially numerically unstable (e.g. finite difference derivative approximation) or ill-defined (e.g. inner product between functions at different resolutions). This is highlighted in our derivation of a fast two-stage approach to performing multidimensional FPCA using the estimated MPB.

The rest of the paper is organized as follows. In Section 2, we formulate the optimal MPB system and analyze its theoretic approximation properties. We then derive an efficient estimation procedure based on the CPD of  $\widehat{\mathcal{G}}$ , the reduced data tensor. Incorporation of roughness-based regularization is also discussed in this section. In Section 3, a procedure for conducting a two-stage FPCA is proposed. Section 4 compares the proposed method with competing methods in simulation studies. In Section 5, we analyze a set of brain imaging data collected from subjects who suffered from traumatic brain injury and healthy controls. Section 6 offers concluding remarks and potential future directions.

## 2 Marginal Product Function Estimation

In this study, we are interested in modeling real-valued square integrable multivariate functions  $u(\mathbf{x}) \in \mathcal{H} := \mathbb{L}^2(\mathcal{M})$ . Here  $\mathbf{x} = (x_1, \dots, x_D)' \in \mathcal{M}$ ; each  $x_d$ , for  $d = 1, \dots, D$ , is a member in the marginal domain  $\mathcal{M}_d$ , which is assumed to be a compact subset of Euclidean space  $\mathbb{R}^{p_d}$ ; and the joint domain of  $u(\mathbf{x})$  can be decomposed as  $\mathcal{M} = \mathcal{M}_1 \times \dots \times \mathcal{M}_D$ .

Let  $H_d := \mathbb{L}^2(\mathcal{M}_d)$ , it is clear that  $\mathcal{H} := \mathbb{L}^2(\mathcal{M}) = \bigotimes_{d=1}^D H_d$ , the tensor product of  $D$  member spaces. We assume that there is a pre-defined complete basis system,  $\phi_d := \{\phi_{d,j}\}_{j=1}^\infty$ , for each marginal functional space  $H_d$ . Denote their rank- $m_d$  truncations as  $\phi_{m_d,d} = (\phi_{d,1}, \dots, \phi_{d,m_d})'$ ;  $H_{m_d,d} := \text{span}(\phi_{m_d,d})$ ; and  $\mathcal{H}_m := \bigotimes_{d=1}^D H_{m_d,d}$ . Here  $\mathbf{m} = (m_1, \dots, m_D)'$  is the collection of  $m_d$  which determines the expressiveness of the truncated basis systems of the member spaces.

By construction,

$$\begin{aligned} \boldsymbol{\tau} &:= \bigotimes_{d=1}^D \phi_d = \left\{ \tau_{j_1, \dots, j_D}(\mathbf{x}) = \prod_{d=1}^D \phi_{d,j_d}(x_d), j_d = 1, \dots, \infty \right\}, \\ \boldsymbol{\tau}_m &:= \bigotimes_{d=1}^D \phi_{m_d,d} = \left\{ \tau_{j_1, \dots, j_D}(\mathbf{x}) = \prod_{d=1}^D \phi_{d,j_d}(x_d), j_d = 1, \dots, m_d \right\} \end{aligned} \quad (1)$$

are the complete tensor product bases for  $\mathcal{H}$  and  $\mathcal{H}_m$ , respectively. Let  $u = \sum_{j_1, \dots, j_D} a_{j_1, \dots, j_D} \phi_{j_1, \dots, j_D}$  and  $v = \sum_{j'_1, \dots, j'_D} b_{j'_1, \dots, j'_D} \phi_{j'_1, \dots, j'_D}$  be two elements in  $\mathcal{H}$ . Their inner product can be represented as follows

$$\langle u, v \rangle_{\mathcal{H}} := \sum_{j_1, \dots, j_D} \sum_{j'_1, \dots, j'_D} \left[ a_{j_1, \dots, j_D} b_{j'_1, \dots, j'_D} \prod_{d=1}^D \langle \phi_{d,j_d}, \phi_{d,j'_d} \rangle_{H_d} \right]. \quad (2)$$

**Definition 2.1** (Marginal product structure). We define  $\zeta \in \mathcal{H}$  to be a rank-1 marginal product function (MPF), or simply an MPF if there is no ambiguity, if it is *multiplicatively separable*:

$$\zeta(\mathbf{x}) = \prod_{d=1}^D \xi_d(x_d), \quad \xi_d \in H_d. \quad (3)$$

As an extension,  $u(\mathbf{x}) \in \mathcal{H}$  is called a rank- $K$  marginal product function ( $K$ -MPF), or it has a rank- $K$  *marginal product structure*, if it is a linear combination of  $K$  linearly independent rank-1 MPFs

$$u(\mathbf{x}) = \sum_{k=1}^K b_k \zeta_k(\mathbf{x}) = \sum_{k=1}^K b_k \prod_{d=1}^D \xi_{k,d}(x_d), \quad \xi_{k,d} \in H_d, \quad b_k \in \mathbb{R}. \quad (4)$$

For convenience, we denote the collection of all rank-1 MPFs generated by the truncated bases as

$$\mathcal{L}_{\mathbf{m}} := \left\{ \zeta(\mathbf{x}) : \zeta(\mathbf{x}) = b \prod_{d=1}^D \xi_d(x_d), \xi_d \in H_{m_d,d}, \|\xi_d\|_{H_d} = 1 \right\} \quad (5)$$

Note that the unit norm condition  $\|\xi_d\|_{H_d} = 1$  is needed to resolve potential identifiability issues. Based on this condition and Equation (2), it can be shown that  $b = \|\zeta\|_{\mathcal{H}}$ . Likewise, let  $\mathcal{L}_{\mathbf{m},K}$  be the set of  $K$ -MPFs generated by functions  $\xi_d \in H_{m_d,d}$

$$\mathcal{L}_{\mathbf{m},K} := \bigcup_{\zeta} \text{span}(\zeta), \quad \zeta = (\zeta_1, \dots, \zeta_K)', \quad \zeta_k \in \mathcal{L}_{\mathbf{m}}. \quad (6)$$

In other words, every  $u(\mathbf{x}) \in \mathcal{L}_{\mathbf{m},K}$  has the following explicit decomposition

$$\begin{aligned} u(\mathbf{x}) &= \sum_{k=1}^K b_k \zeta_k(\mathbf{x}) = \sum_{k=1}^K b_k \left[ \prod_{d=1}^D \left( \sum_{j=1}^{m_d} c_{k,d,j} \phi_{d,j}(x_d) \right) \right]. \\ \zeta_k(\mathbf{x}) &= \prod_{d=1}^D \xi_{k,d}(x_d), \quad \xi_{k,d}(x_d) = \sum_{j=1}^{m_d} c_{k,d,j} \phi_{d,j}(x_d), \quad \|\xi_{k,d}\|_{H_d} = 1. \end{aligned} \quad (7)$$

Several useful theoretical results about MPB are presented in the following subsections. Their proofs can be found in Section S1 of the Supplementary Materials.

## 2.1 Approximation Theory

In the case of deterministic functions, convergence rates for optimal rank  $K$  approximations have been derived under various scenarios (Temlyakov, 2003; Barron et al., 2008). In the context of random functions, it is easy to show that the expected integrated squared error for representing realizations with the first  $K$  eigenfunctions is dictated by the decay rate of the spectrum of the covariance operator. In this section, we contribute to these results by analyzing the convergence rate of the optimal rank- $K$  MPB for representing realizations of a random function.

Without loss of generality, for clarity of the presentation of the following analysis we assume that  $m_d \equiv m$  for all  $d = 1, \dots, D$ , so that we can replace the integer vector  $\mathbf{m}$  in all notations by a single integer  $m$ . We also assume the Lebesgue measure of  $\mathcal{M}$  is 1.

*Assumption 1.* Let  $U$  be a random function with realizations in  $\mathcal{H}$ , i.e. a measurable mapping from some probability space  $(\Omega, \sigma(\Omega), \mathbb{P}) \rightarrow (\mathcal{H}, \mathcal{B}(\mathcal{H}))$ . Assume that  $\mathbb{E}_{\mathbb{P}}[U] = 0$ , and it has

finite second order moment:  $\mathbb{E}_{\mathbb{P}}[\int_{\mathcal{M}} U^2(\mathbf{x})d\mathbf{x}] < \infty$ . We also assume that  $U$  is *mean-square continuous*, that is, for any  $\mathbf{x} \in \mathcal{M}$  and any sequence  $\{\mathbf{x}_n\}$  in  $\mathcal{M}$  converging to  $\mathbf{x}$ , then

$$\lim_{n \rightarrow \infty} \mathbb{E}_{\mathbb{P}} [(U(\mathbf{x}_n) - U(\mathbf{x}))^2] = 0.$$

The mean zero assumption on  $U$  is made for convenience of presentation and would not fundamentally change any of our results. The mean square integrability and mean-square continuity assumptions are a standard requirement (Hsing and Eubank, 2015). Note that under Assumption 1, we are guaranteed that the covariance function  $C(\mathbf{x}, \mathbf{y}) := \mathbb{E}_{\mathbb{P}} [U(\mathbf{x})U(\mathbf{y})]$  is continuous on  $\mathcal{M} \times \mathcal{M}$ . By Mercer's theorem, this covariance function has an eigen-decomposition  $C(\mathbf{x}, \mathbf{y}) = \sum_{k=1}^{\infty} \rho_k \psi_k(\mathbf{x})\psi_k(\mathbf{y})$ , where  $\{\psi_k\}_{k=1}^{\infty}$  forms a complete orthonormal sequence of eigenfunctions in  $\mathcal{H}$  and  $\{\rho_k\}_{k=1}^{\infty}$  is a non-increasing sequence of real, non-negative eigenvalues. Additionally, by the Karhunen-Loéve theorem, with probability one we have the decomposition  $U(\mathbf{x}) = \sum_{k=1}^{\infty} Z_k \psi_k(\mathbf{x})$ , where  $Z_k = \langle U, \psi_k \rangle_{\mathcal{H}}$ , which are mean zero random variables with  $\mathbb{E}_P[Z_k Z_j] = \rho_k \delta_{kj}$ .

We want to analyze the performance of the best basis of  $K$ -MPFs for representing realizations of  $U$ , a notion formalized as follows:

**Definition 2.2** (Optimal Rank- $K$  MPB). Denote the set of linearly independent  $K$ -MPFs

$$\mathcal{V}_{m,K} := \left\{ \boldsymbol{\zeta} = (\zeta_1, \dots, \zeta_K)' : \zeta_k \in \mathcal{L}_m, \zeta_1, \dots, \zeta_K \text{ linearly independent} \right\}, \quad (8)$$

where it is assumed that  $K \leq m^D$ . For any  $\boldsymbol{\zeta} \in \mathcal{V}_{m,K}$ , denote the oracle least squares estimator

$$u^*(\boldsymbol{\zeta}) = \min_{u \in \text{span}(\boldsymbol{\zeta})} \|U - u\|_{\mathcal{H}}^2 \quad (9)$$

The optimal rank- $K$  MPB, denoted  $K$ -oMPB, is defined as the solution to

$$\boldsymbol{\zeta}^* = \arg \inf_{\boldsymbol{\zeta} \in \mathcal{V}_{m,K}} \mathbb{E} \|U - u^*(\boldsymbol{\zeta})\|_{\mathcal{H}}^2 \quad (10)$$

Clearly,  $\text{span}(\boldsymbol{\zeta}^*) \subset \mathcal{L}_{m,K}$  and therefore the  $K$ -oMPB can be interpreted as the element in the collection of rank- $K$  approximation spaces best adapted to representing realizations of  $U$ , in the least squares sense. Before investigating its performance, we make the following observation:

**Proposition 2.1.** *If  $K = m^D$  then  $\text{span}(\zeta^*) = \mathcal{L}_{m,K} = \mathcal{H}_m$ .*

As a direct consequence, if we make no further assumptions about the distribution of  $U$ , at worst we can expect the approximation properties of the  $K$ -oMPB to behave like the associated tensor product basis system. This allows us to conclude a universal approximation property for (10) as  $m \rightarrow \infty$ , i.e. inherited from the tensor product basis. Unfortunately we make no headway in our aim to combat the curse of dimensionality, as in proposition 2.1  $K$  grows exponentially in  $D$ . To illustrate the potential for the MPF structure to avoid the curse of dimensionality, we analyze the rate of convergence of (10) as a function of the *marginal* and *global ranks*,  $m$  and  $K$ , respectively. Note that the accuracy of this approximation will depend on the convergence rate of both the chosen marginal basis systems  $\phi_d$  as well as the tail-sum of the eigenvalues of  $C(\mathbf{x}, \mathbf{y})$ .

**Definition 2.3.** Let the function  $w_{\phi_d}(m)$  be the  $\mathbb{L}^2(\mathcal{M}_d)$  convergence rate of the  $d$ th marginal basis system  $\phi_d$  and  $w_{\tau_m}(m)$  be the  $\mathbb{L}^2(\mathcal{M})$  convergence rate of the tensor product basis system  $\tau_m$ . That is, for any  $f_d \in \mathcal{H}_d$ ,  $f \in \mathcal{H}$

$$\left\| P_{\mathcal{H}_{m,d}^\perp}(f_d) \right\|_{\mathcal{H}_d} = O(w_{\phi_d}(m)), \quad \left\| P_{\mathcal{H}_m^\perp}(f) \right\|_{\mathcal{H}} = O(w_{\tau_m}(m))$$

where  $P_{\mathcal{H}_{m,d}^\perp}$ ,  $P_{\mathcal{H}_m^\perp}$  are the projection operators onto  $\mathcal{H}_{m,d}^\perp$  and  $\mathcal{H}_m^\perp$ , the orthogonal complements of  $\mathcal{H}_{m,d}$  in  $\mathcal{H}_d$  and  $\mathcal{H}_m$  in  $\mathcal{H}$ , respectively.

**Definition 2.4.** Let the function  $h(K)$  be convergence rate of the tail-sum of the eigenvalues of the covariance operator associated with  $C(\mathbf{x}, \mathbf{y})$ , that is

$$\sum_{k=K+1}^{\infty} \lambda_k = O(h(K))$$

Because  $\phi_d$  is a complete basis of  $\mathcal{H}_d$  and  $U$  has finite variance, both  $w_{\tau_m}(m)$  and  $h(K)$  must converge to zero with at least rate  $o(1)$ . In practice, we can get better rates of convergence with some additional assumptions. For example, it may be reasonable to assume that eigenfunctions (hence the covariance function) are relatively smooth (e.g., differentiable) and  $U$  has higher order moments (e.g., finite skewness) for a large class of models. In this case,  $w_{\tau_m}(m)$  and  $h(K)$  converge to zero at polynomial rates, which are much faster than the generic  $o(1)$  rate. That said, we leave them generic in our analysis as to accommodate

multiple decay rates and smoothness classes of covariance function. The following two definitions describe objects required for the statement of main result.

**Definition 2.5.** Let  $\mathcal{A}_k$  be the the  $D$ -mode tensor with elements  $\mathcal{A}_k(j_1, \dots, j_D)$  defined by

$$P_{\mathcal{H}_m}(\psi_k) = \sum_{j_1=1}^m \cdots \sum_{j_D=1}^m \mathcal{A}_k(j_1, \dots, j_D) \phi_{1,j_1} \cdots \phi_{D,j_D},$$

where  $P_{\mathcal{H}_m}$  is the projection operator onto  $\mathcal{H}_m$ .

**Definition 2.6.** Let  $\mathbf{J}_{\phi_d}$  be the matrix of pairwise  $\mathcal{H}_{m,d}$  inner products of  $\phi_{m,d}$ . Define the inner product space  $(\bigotimes_{d=1}^D \mathbb{R}^m, \langle \cdot, \cdot \rangle_{\tilde{F}})$ , where

$$\begin{aligned} \langle \mathcal{T}_1, \mathcal{T}_2 \rangle_{\tilde{F}} &= \langle \mathcal{T}_1, \mathcal{T}_2 \times_1 \mathbf{J}_{\phi_1} \cdots \times_D \mathbf{J}_{\phi_D} \rangle_F \equiv \langle \mathcal{T}_1 \times_1 \mathbf{J}_{\phi_1} \cdots \times_D \mathbf{J}_{\phi_D}, \mathcal{T}_2 \rangle_F \\ &= \sum_{i_1=1}^m \cdots \sum_{i_D=1}^m \sum_{j_1=1}^m \cdots \sum_{j_D=1}^m \mathcal{T}_1(i_1, \dots, i_D) \mathcal{T}_2(j_1, \dots, j_D) \prod_{d=1}^D \mathbf{J}_{\phi_d}(i_d, j_d) \end{aligned}$$

for tensors  $\mathcal{T}_1, \mathcal{T}_2 \in \bigotimes_{d=1}^D \mathbb{R}^m$ .

As a remark, “ $\times_d$ ” is called  $d$ -mode multiplication in tensor algebra. See e.g. Kolda and Bader (2009) for more details about this operation.  $\langle \mathcal{T}_1, \mathcal{T}_2 \rangle_{\tilde{F}}$  can be considered as a weighted version of the Frobenius inner product. We are now ready to state our main result on the approximation properties of the  $K$ -oMPB.

**Theorem 2.2.** *Define the parameter space*

$$\mathcal{C}_{m,K} := \left\{ \mathbf{c}_{d,k} \in \mathbb{R}^m : \mathbf{c}'_{d,k} \mathbf{J}_{\phi_d} \mathbf{c}_{d,k} = 1, \mathbf{c}_{d,1}, \dots, \mathbf{c}_{d,K} \text{ linearly independent for } d = 1, \dots, D \right\},$$

and the  $K$ -vector

$$\mathbf{b}_l^* = \begin{pmatrix} \prod_{d=1}^D \mathbf{c}'_{d,1} \mathbf{J}_{\phi_d} \mathbf{c}_{d,1} & \prod_{d=1}^D \mathbf{c}'_{d,1} \mathbf{J}_{\phi_d} \mathbf{c}_{d,2} & \cdots & \prod_{d=1}^D \mathbf{c}'_{d,1} \mathbf{J}_{\phi_d} \mathbf{c}_{d,K} \\ \prod_{d=1}^D \mathbf{c}'_{d,2} \mathbf{J}_{\phi_d} \mathbf{c}_{d,1} & \prod_{d=1}^D \mathbf{c}'_{d,2} \mathbf{J}_{\phi_d} \mathbf{c}_{d,2} & \cdots & \\ \vdots & & \ddots & \\ \prod_{d=1}^D \mathbf{c}'_{d,K} \mathbf{J}_{\phi_d} \mathbf{c}_{d,1} & \cdots & & \prod_{d=1}^D \mathbf{c}'_{d,K} \mathbf{J}_{\phi_d} \mathbf{c}_{d,K} \end{pmatrix}^{-1} \begin{bmatrix} \langle \mathcal{A}_l, \bigotimes_{d=1}^D \mathbf{c}_{d,1} \rangle_{\tilde{F}} \\ \langle \mathcal{A}_l, \bigotimes_{d=1}^D \mathbf{c}_{d,2} \rangle_{\tilde{F}} \\ \vdots \\ \langle \mathcal{A}_l, \bigotimes_{d=1}^D \mathbf{c}_{d,K} \rangle_{\tilde{F}} \end{bmatrix}.$$

Under Assumption (1),

$$\begin{aligned} \inf_{\zeta \in \mathcal{V}_{m,K}} \mathbb{E} \|U - u^*(\zeta)\|_{\mathcal{H}}^2 &= \inf_{\mathbf{c}_{d,k} \in \mathcal{C}_{m,K}} \sum_{l=1}^K \rho_l \left\| \mathcal{A}_l - \sum_{k=1}^K b_{l,k}^* \bigotimes_{d=1}^D \mathbf{c}_{d,k} \right\|_{\tilde{F}}^2 + \\ &O(h(K)) + O(w_{\tau_m}(m)), \end{aligned} \quad (11)$$

where  $b_{l,k}^*$  is the  $k$ th element of  $\mathbf{b}_l^*$ .

Note that the independence of the  $\mathbf{c}_{d,k}$ 's guarantees that the matrix of inner products in the definition of  $\mathbf{b}_l^*$  is invertible. The  $O(h(K))$  and  $O(w_{\tau_m}(m))$  terms in Equation (11) quantify the irreducible contributions to the expected error resulting from the finite truncation of the global and marginal ranks. It is then the first term, which defines a joint tensor rank decomposition under the  $\|\cdot\|_{\bar{F}}$  metric with weights determined by the variance of the corresponding components, that drives the performance of the  $K$ -oMPB. Heuristically, this term quantifies the degree to which the leading modes of functional variation can be jointly represented using a basis system of MPFs, which clearly will depend heavily on the properties of the distribution of  $U$ . That said, Theorem 2.2 can be used to derive more exact results if further structure is assumed on  $U$ . To illustrate this point, Corollary 2.3 shows the results under an additional assumption on the  $\psi_k$ 's.

**Corollary 2.3.** *Assume that the eigenfunctions  $\psi_k$  are rank-1 MPF, i.e. they are multiplicatively separable. Under Assumption (1), we have*

$$\inf_{\zeta \in \mathcal{V}_{m,K}} \mathbb{E} \|U - u^*(\zeta)\|_{\mathcal{H}}^2 = O\left(K^2 \prod_{d=1}^D w_{\phi_d}(m)\right) + O(h(K)) \quad (12)$$

Since we assume  $K = O(m^D)$ , in order to guarantee (12) to be  $o(1)$ , it must be the case that  $O(\prod_{d=1}^D m^2 w_{\phi_d}(m)) = o(1)$ , i.e.  $w_{\phi_d}(m) < m^{-2}$ , which is satisfied for many reasonable choices of basis system and marginal smoothness assumptions on the eigenfunctions.

The separability assumption in Corollary 2.3 indicates that the eigenfunctions are in  $\bigcup_{m \rightarrow \infty} \mathcal{V}_{m,K}$ . In this special case, the  $K$ -oMPB is equivalent to the leading  $K$  eigenfunctions, hence the convergence rate only depends on the irreducible error from the finite truncation of the marginal basis and the tail-sum rate of the spectrum. This assumption may seem difficult to verify in general, but a sufficient condition is that the covariance function is separable, i.e.  $C(\mathbf{x}, \mathbf{y}) = \prod_{d=1}^D C_d(x_d, y_d)$  for some appropriately defined marginal covariance functions  $C_d$ , see Lemma S5 of the Supplementary Material. Theorem 2.2 can be used to facilitate the analysis of convergence rates of  $K$ -oMPB under alternative structures on  $C(\mathbf{x}, \mathbf{y})$ , and hence the eigenfunctions, e.g. the popular single-spike model, though we leave this to a future work.

## 2.2 Estimation

### 2.2.1 Statistical Model

Assume that a random sample of  $N$  realizations  $u_i \sim U$  are observed on a common grid

$$\mathcal{X} = (x_{11}, x_{12}, \dots, x_{1n_1})' \times (x_{21}, x_{22}, \dots, x_{2n_2})' \times \cdots \times (x_{D1}, x_{D2}, \dots, x_{Dn_D})'$$

contaminated with *i.i.d.* measurement errors, where each vector of marginal grid points  $\mathbf{x}_d := (x_{d1}, x_{d2}, \dots, x_{dn_d}) \in \mathcal{M}_d$ . The observations are arranged into a  $(D + 1)$ -mode tensor with dimensions  $(n_1, n_2, \dots, n_D, N)$ , denoted as  $\mathcal{Y}$ , where

$$\mathcal{Y}(i_1, i_2, \dots, i_D, i) = u_i(x_{1,i_1}, x_{2,i_2}, \dots, x_{D,i_D}) + \mathcal{E}(i_1, i_2, \dots, i_D, i) \quad (13)$$

for  $i_d = 1, 2, \dots, n_d$ ,  $d = 1, 2, \dots, D$ , and  $i = 1, 2, \dots, N$ ; where  $\mathbb{E}[\text{vec}(\mathcal{E})] = \mathbf{0}$  and  $\text{Var}[\text{vec}(\mathcal{E})] = \sigma^2 \mathbf{I}$ . For convenience, denote the observed data tensor for the  $i$ th subject as  $\mathcal{Y}_i \in \mathbb{R}^{n_1 \times \cdots \times n_D}$ .

### 2.2.2 Marginal Product Functional Representation

We begin with defining some quantities of interest. Let  $\Phi_d \in \mathbb{R}^{n_d \times m_d}$  be the evaluation of  $\phi_d$  on the marginal grid  $\mathbf{x}_d$ , i.e.  $\Phi_{d,i_d j_d} := \phi_{d,j_d}(x_{d,i_d})$ , and let  $\Phi_d = \mathbf{U}_d \mathbf{D}_d \mathbf{V}_d'$  be the SVD of these matrices. In general, we have  $n_d > m_d$ , so  $\mathbf{U}_d \in \mathbb{R}^{n_d \times m_d}$  is a semi-orthogonal matrix;  $\mathbf{D}_d \in \mathbb{R}^{m_d \times m_d}$  is an invertible diagonal matrix; and  $\mathbf{V}_d \in \mathbb{R}^{m_d \times m_d}$  is an orthogonal matrix. We can write the evaluation of the MPB functions  $\xi_d = (\xi_{d1}, \dots, \xi_{dK})'$  on  $\mathbf{x}_d$ , denoted  $\Xi_d \in \mathbb{R}^{n_d \times K}$ , as

$$\Xi_d = \Phi_d \mathbf{C}_d = \mathbf{U}_d \mathbf{D}_d \mathbf{V}_d' \mathbf{C}_d = \mathbf{U}_d \tilde{\mathbf{C}}_d, \quad \tilde{\mathbf{C}}_d := \mathbf{D}_d \mathbf{V}_d' \mathbf{C}_d.$$

Here  $\mathbf{C}_d \in \mathbb{R}^{m_d \times K}$  and its columns are  $\mathbf{c}_{d,k}$ , the coefficients of the representation of  $\xi_{d,k}$  over  $\phi_d$ .

Clearly, computing the  $K$ -oMPB using Equation (11) requires unknown oracle information. Since we assume access to discrete, noisy observations of  $u_i$ , we must work with minimizing an empirical formulation of (10), given by

$$(\hat{\mathbf{C}}_1, \dots, \hat{\mathbf{C}}_D, \hat{\mathbf{B}}) = \min_{\mathbf{C}_1, \dots, \mathbf{C}_D, \mathbf{B}} \sum_{i=1}^N \left\| \mathcal{Y}_i - \sum_{k=1}^K \mathbf{B}_{i,k} \bigotimes_{d=1}^D \Phi_d \mathbf{c}_{d,k} \right\|_F^2. \quad (14)$$

where  $\mathbf{B} \in \mathbb{R}^{N \times K}$  is the matrix of coefficients for the  $\zeta_k$ 's for each of the  $N$  samples. The following theorem proves the equivalence between the solution of Equation (14) and the rank- $K$  CPD of an appropriately defined tensor.

**Theorem 2.4** (Functional Tensor Decomposition Theorem). *Define  $\widehat{\mathcal{G}} := \mathcal{Y} \times_1 \mathbf{U}'_1 \times_2 \mathbf{U}'_2 \cdots \times_D \mathbf{U}'_D$ , which is a  $(D+1)$ -mode tensor with dimensions  $(m_1, m_2, \dots, m_D, N)$  and denote its rank- $K$  decomposition by  $\widehat{\mathcal{G}}_K(\check{\mathbf{B}}, \check{\mathbf{C}}) = \sum_{k=1}^K \left[ \bigotimes_{d=1}^D \check{\mathbf{c}}_{d,k} \right] \otimes \check{\mathbf{b}}_k$ , with factor matrices  $\check{\mathbf{B}} \in \mathbb{R}^{N \times K}$  and  $\check{\mathbf{C}} = [\check{\mathbf{C}}_1, \dots, \check{\mathbf{C}}_D]$ ,  $\check{\mathbf{C}}_d \in \mathbb{R}^{m_d \times K}$ .  $\check{\mathbf{c}}_{d,k}$  and  $\check{\mathbf{b}}_k$  are the  $k$ th column of  $\check{\mathbf{C}}_d$  and  $\check{\mathbf{B}}$ , respectively. The optimization problem (14) has the following solutions:  $\widehat{\mathbf{B}} = \check{\mathbf{B}}$  and  $\widehat{\mathbf{C}}_d = \mathbf{V}_d \mathbf{D}_d^{-1} \check{\mathbf{C}}_d$ , for  $d = 1, \dots, D$ .*

**Corollary 2.5.** *As a special case, if  $D = 2$  and  $N = 1$ , i.e. single subject on a product of 2-marginal domains,  $\widehat{\mathbf{C}}_d = \mathbf{V}_d \mathbf{D}_d^{-1} \Sigma^{1/2} \mathbf{Q}_d$ , where  $\mathbf{Q}_d \Sigma \mathbf{Q}'_d$  is the singular value decomposition of  $\mathbf{Y} \times_1 \mathbf{U}'_1 \times \mathbf{U}'_2 = \mathbf{U}'_1 \mathbf{Y} \mathbf{U}_2$ .*

Theorem 2.4 shows that obtaining the empirical estimate of the  $K$ -oMPB and corresponding subject coefficient estimates is equivalent to the CPD of the  $\widehat{\mathcal{G}}$  tensor. Recall that the dimensionality of  $\widehat{\mathcal{G}}$  is  $m_1 \times \cdots \times m_D$ , which is controlled by the user and can often be made much smaller than that of  $\mathcal{Y}$  in practice. Consequently, Theorem 2.4 offers a tunable, more efficient way to represent tensor-valued data into multidimensional functions than the alternative decompose-then-represent approach.

We offer the following intuitive interpretation for Theorem 2.4. Let  $\mathcal{U} \in \mathbb{R}^{n_1 \times \cdots \times n_D \times N}$  be the tensor of evaluations of the sample realizations of  $(u_1, \dots, u_N)$ , thus  $\mathcal{Y} = \mathcal{U} + \mathcal{E}$ . Applying the sequence of  $d$ -mode multiplications to both side of the equality, we see that

$$\begin{aligned} \widehat{\mathcal{G}} &= \mathcal{Y} \times_1 \mathbf{U}'_1 \times_2 \mathbf{U}'_2 \cdots \times_D \mathbf{U}'_D \\ &= \mathcal{U} \times_1 \mathbf{U}'_1 \times_2 \mathbf{U}'_2 \cdots \times_D \mathbf{U}'_D + \mathcal{E} \times_1 \mathbf{U}'_1 \times_2 \mathbf{U}'_2 \cdots \times_D \mathbf{U}'_D \\ &\equiv \mathcal{G} + \widehat{\mathcal{E}}, \quad \widehat{\mathcal{E}} := \mathcal{E} \times_1 \mathbf{U}'_1 \times_2 \mathbf{U}'_2 \cdots \times_D \mathbf{U}'_D. \end{aligned}$$

Since  $\mathcal{E}$  is a tensor of *i.i.d.* errors (isotropic) and  $\mathbf{U}_d$  are semi-orthogonal matrices,  $\widehat{\mathcal{E}}$  is also isotropic. Therefore the rank- $K$  decomposition of  $\widehat{\mathcal{G}}$  is the best estimate of the rank- $K$  decomposition of  $\mathcal{G}$  from the data.

We now turn our attention to interpreting the tensor  $\mathcal{G}$ . The columns of  $\mathbf{U}_d$  form an orthonormal basis for an  $m_d$ -dimensional linear subspace of  $\mathbb{R}^{n_d}$ , call it  $R_d$ . This corresponds to the regression subspace for  $\Phi_d$ , i.e. the linear span of the evaluation of the basis system  $\phi_d$  over the  $d$ th marginal coordinate grid  $\mathbf{x}_d$ . Consider the definition of  $d$ -mode multiplication in terms of the more familiar matrix multiplication

$$\mathcal{U} \times_d \mathbf{U}'_d = \mathcal{T} \iff \mathcal{T}_{(d)} = \mathbf{U}'_d \mathcal{U}_{(d)},$$

where  $\mathcal{T}$  is a tensor and  $\mathcal{T}_{(d)}$  is the  $d$ -mode unfolding of  $\mathcal{T}$ , obtained by stacking all the mode- $d$  vectors into the columns of a matrix. Now, the matrix multiplication  $\mathbf{U}'_d \mathcal{U}_{(d)}$  corresponds to a coordinate transformation along the  $d$ th dimension to an orthogonal basis spanning  $R_d$ . Since  $\mathcal{G}$  is obtained by a sequence of such transformations onto the product space  $R_1 \otimes R_2 \cdots \otimes R_D$ , the subject mode slices  $\mathcal{G}_i$  are an estimate of a *transformation of the coefficient tensor* for subject  $i$  with respect to the tensor product basis  $\boldsymbol{\tau}_m$ .

### 2.2.3 Regularization

It is often desirable to incorporate regularization into the estimation of the function representations to ameliorate the influence of noise and promote “smoother” solutions. In this work, we promote smoothness in the estimated  $K$ -oMPB basis by adding a non-negative penalty functional to the objective function in Equation (14). We make the following assumption on this penalty:

*Assumption 2* (Separable Roughness Penalty Functional). Denote the Sobolev space over the  $d$ th marginal domain  $\mathbb{W}^{\alpha_d,2}(\mathcal{M}_d)$  for some order  $\alpha_d$ , and we assume that  $u_d(x_d) \in \mathbb{W}^{\alpha_d,2}(\mathcal{M}_d)$ . For any  $u(\mathbf{x}) = u_1(x_1) \cdots u_D(x_D) \in \mathbb{W}^{\alpha_1,2}(\mathcal{M}_1) \times \cdots \times \mathbb{W}^{\alpha_D,2}(\mathcal{M}_D)$ , we assume that the penalty functional  $\text{Pen} : \mathbb{W}^{\alpha_1,2}(\mathcal{M}_1) \times \cdots \times \mathbb{W}^{\alpha_D,2}(\mathcal{M}_D) \rightarrow [0, \infty)$  can be represented as

$$\text{Pen}(u) = \int_{\mathcal{M}} \sum_{d=1}^D \lambda_d L_d^2(u_d)$$

for some  $\lambda_d > 0$ , where  $L_d : \mathbb{W}^{\alpha_d,2}(\mathcal{M}_d) \rightarrow \mathbb{L}^2(\mathcal{M}_d)$  is a linear (partial) differential operator, with order  $\alpha_d$  defined appropriately.

Clearly, in order to apply  $\text{Pen}(u)$  to the candidate MPB, we must assume that  $\xi_{k,d} \in \mathbb{W}^{\alpha_d,2}(\mathcal{M}_d)$ . We penalize the total roughness for a set of  $K > 1$  basis functions by summing

the contribution from each  $\zeta_k$ . Considering the representation of  $\xi_{k,d}$  with respect to the marginal basis  $\phi_d$ , we have the following result.

**Proposition 2.6.** *Consider the basis expansion  $\xi_{k,d}(x_d) = \sum_{j=1}^{m_d} \mathbf{C}_{d,jk} \phi_{d,j}(x_d)$ . There exists a symmetric positive semi-definite matrix  $\mathbf{T}_d$ , depending on  $L_d$  and  $\phi_d$ , such that*

$$\sum_{k=1}^K \int_{\mathcal{M}_d} L_d^2(\xi_{k,d}) = \text{tr}(\tilde{\mathbf{C}}_d' \mathbf{T}_d \tilde{\mathbf{C}}_d),$$

where  $\tilde{\mathbf{C}}_d = \mathbf{D}_d \mathbf{V}_d' \mathbf{C}_d$ .

As a result, we have that penalties of the form of Assumption 2 are quadratic in the transformed coordinate matrices  $\tilde{\mathbf{C}}_d$  and therefore convex. Coupled with separability, this permits the derivation of efficient numerical algorithms to estimate the optimal MPB functions, which will be discussed in Section 2.3.

We also incorporate penalization on the coefficient matrix  $\mathbf{B}$  using the penalty function denoted  $l(\mathbf{B})$ . We assume that  $l(\mathbf{B})$  is convex, which is a requirement to guarantee the convergence of the algorithm in Section 2.3, but otherwise leave its form unspecified. For example, common choices such as lasso and ridge penalties can be seamlessly integrated. In any case, the resulting regularized augmentation of Equation (14) can be written as

$$\min_{\mathbf{C}_1, \dots, \mathbf{C}_D, \mathbf{B}} \sum_{i=1}^N \left\| \mathcal{Y}_i - \sum_{k=1}^K \mathbf{B}_{ik} \bigotimes_{d=1}^D \Phi_d \mathbf{c}_{d,k} \right\|_F^2 + \sum_{k=1}^K \sum_{d=1}^D \lambda_d \int_{\mathcal{M}_d} L_d^2(\xi_{k,d}) + \lambda_{D+1} l(\mathbf{B}). \quad (15)$$

Using the results from Theorem 2.4 and Proposition 2.6, it is easy to show that the solution to Equation (15) is a linear transformation of the solution to

$$\min_{\mathbf{B}, \tilde{\mathbf{C}}_1, \dots, \tilde{\mathbf{C}}_D} \left\| \hat{\mathcal{G}} - \sum_{k=1}^K \bigotimes_{d=1}^D \tilde{\mathbf{c}}_{d,k} \otimes \mathbf{b}_k \right\|_F^2 + \sum_{d=1}^D \lambda_d \text{tr}(\tilde{\mathbf{C}}_d' \mathbf{T}_d \tilde{\mathbf{C}}_d) + \lambda_{D+1} l(\mathbf{B}), \quad (16)$$

where  $\mathbf{b}_k$  is the  $k$ th column of  $\mathbf{B}$ .

In the following section, we propose an algorithm for approximating the solution to Equation (16), and hence (15).

## 2.3 Algorithm for Estimating $K$ -oMPB

The optimization problem (16) is non-convex and NP-hard (Hillar and Lim, 2013). To derive a computationally tractable approximation algorithm, we propose a block coordinate

descent based approach in which, for the  $(r + 1)$ 'th iteration, the variables are updated according to the sequence of conditional minimization problems

$$\tilde{\mathbf{C}}_d^{(r+1)} = \min_{\mathbf{X}} g(\tilde{\mathbf{C}}_1^{(r+1)}, \dots, \tilde{\mathbf{C}}_{d-1}^{(r+1)}, \mathbf{X}, \tilde{\mathbf{C}}_{d+1}^{(r)}, \dots, \tilde{\mathbf{C}}_D^{(r)}, \mathbf{B}^{(r)}), \quad (17)$$

for  $d = 1, \dots, D$  and likewise for  $\mathbf{B}^{(r+1)}$ , where  $g$  denotes the objective function from (16).

Using the properties of the  $d$ -mode matricization, we can write the conditional minimization problem defining the update of  $\tilde{\mathbf{C}}_d$  as

$$\tilde{\mathbf{C}}_d^{(r+1)} = \min_{\tilde{\mathbf{C}}_d} \|\mathbf{G}'_{(d)} - \tilde{\mathbf{C}}_d \mathbf{W}_d^{(r)'}\|_F^2 + \lambda_d \text{tr}(\tilde{\mathbf{C}}_d' \mathbf{T}_d \tilde{\mathbf{C}}_d). \quad (18)$$

The update for  $\mathbf{B}$  is given by

$$\mathbf{B}^{(r+1)} = \min_{\mathbf{B}} \|\mathbf{G}_{(D+1)} - \mathbf{W}_{D+1}^{(r)} \mathbf{B}'\|_F^2 + \lambda_{D+1} l(\mathbf{B}), \quad (19)$$

where  $\mathbf{W}_d^{(r)} = (\odot_{j<d}^D \tilde{\mathbf{C}}_j^{(r+1)} \odot_{j>d}^D \tilde{\mathbf{C}}_j^{(r)}) \odot \mathbf{B}^{(r)}$  for  $d = 1, \dots, D$ ,  $\mathbf{W}_{D+1}^{(r)} = \odot_{d=1}^D \tilde{\mathbf{C}}_d^{(r+1)}$  and  $\mathbf{G}_{(d)}$  is the  $d$ -mode unfolding of  $\mathcal{G}$ . Here  $\odot$  is the Khatri–Rao product. From here on the superscript  $r$  denoting iteration is dropped for clarity.

It can be shown that the solution to the subproblem (18) is equivalently defined by the solution to

$$\tilde{\mathbf{C}}_d \mathbf{W}_d' \mathbf{W}_d + \lambda_d \mathbf{T}_d \tilde{\mathbf{C}}_d = \mathbf{W}_d' \mathbf{G}_{(d)}. \quad (20)$$

This equivalence can be verified by noting that (20) defines the gradient equations of (18) and that the solution is globally optimum due to convexity. Equation (20) is known as the Sylvester equation and has a unique solution under very mild conditions (specifically  $\mathbf{W}_d' \mathbf{W}_d$  and  $\lambda_d \mathbf{T}_d$  must have no common eigenvalues). Efficient algorithms for solving the Sylvester equation (Bartels and Stewart, 1972; Golub et al., 1979) are readily available in most common numerical computing languages.

We notice that procedure (19) defines (a rescaling) of the so-called *proximal operator* of  $l$ . Since  $l$  is assumed to be convex, optimization problems of this form are strongly convex and therefore have unique minimizer. A globally convergent numerical approximation scheme can be formed using an alternating direction method of multipliers (ADMM) algorithm (Parikh and Boyd, 2014). To derive the ADMM updates, first notice that by introducing

the auxiliary variable  $\mathbf{Z} = \mathbf{B}'$ , the subproblem (19) can be written in separable form as

$$\begin{aligned} \min_{\mathbf{B}, \mathbf{Z}} & \|\mathbf{G}_{(D+1)} - \mathbf{W}_{D+1}\mathbf{Z}\|_F^2 + \lambda_{D+1}l(\mathbf{B}) \\ \text{subject to} & \mathbf{B} - \mathbf{Z}' = \mathbf{0}. \end{aligned} \quad (21)$$

The ADMM then consists of the iterates

$$\mathbf{B}_{\text{update}} \leftarrow \min_{\mathbf{B}} (\lambda_{D+1}l(\mathbf{B}) + \rho\|\mathbf{B} - \mathbf{Z}' + \mathbf{U}^*\|_F^2) \quad (22)$$

$$\mathbf{Z}_{\text{update}} \leftarrow \min_{\mathbf{Z}} (\|\mathbf{G}_{(D+1)} - \mathbf{W}_{D+1}\mathbf{Z}\|_F^2 + \rho\|\mathbf{B} - \mathbf{Z}' + \mathbf{U}^*\|_F^2) \quad (23)$$

$$\mathbf{U}_{\text{update}}^* \leftarrow \mathbf{U}^* + \mathbf{B} - \mathbf{Z}' \quad (24)$$

for some choice of  $\rho > 0$ , where  $\mathbf{U}^*$  is the scaled dual variable associated with the constraint.

The update (23) is a matrix ridge regression and has analytic solution given by

$$\mathbf{Z}_{\text{update}} = [\mathbf{W}'_{D+1}\mathbf{W}_{D+1} + \rho\mathbf{I}]^{-1}[\mathbf{W}'_{D+1}\mathbf{G}_{(D+1)} + \rho(\mathbf{B} + \mathbf{U}^*)']. \quad (25)$$

Clearly, the solution to the update (22) will depend on the exact form of  $l$ , but it can be shown that many reasonable choices permit an analytic form. For example, if  $l(\cdot) = \|\cdot\|_1$ , the update is given by the *element-wise soft thresholding operator* applied to matrix  $\mathbf{Z}' - \mathbf{U}^*$ .

Algorithm 1 provides pseudocode for the proposed block coordinate descent scheme. For the ADMM subproblem, we adopt the stopping criteria proposed in Boyd et al. (2011) based on the primal and dual residuals at the  $r^{\text{th}}$  iteration, which in our problem have the form

$$r_{\text{primal}}^{(r)} = \|\mathbf{B}^{(r)} - \mathbf{Z}^{(r)'}\|_F, \quad r_{\text{dual}}^{(r)} = \|\rho(\mathbf{Z}^{(r)} - \mathbf{Z}^{(r-1)})\|_F. \quad (26)$$

To guarantee the convergence of Algorithm 1 to a stationary point of  $g$  and improve performance, an additional proximal regularization can be added to (17). For brevity, we omit discussion of this here and refer the interested reader to Section S2 in Supplementary Text.

We conclude this section with a few brief remarks related to practical considerations in the implementation of Algorithm 1. The matrix products  $\mathbf{W}'_d\mathbf{W}_d$  and  $\mathbf{W}'_d\mathbf{G}_{(d)}$  can become computationally expensive when  $D$  and/or  $m_d$  become sufficiently large. To combat this potential computational bottleneck, the former can be calculated efficiently without explicitly constructing the associated Khatri-Rao product by leveraging the identity  $[\odot_i A_i]'[\odot_i A_i] =$

$\circ_i A'_i A_i$ , where  $\circ$  is the Hadamard product. The product  $\mathbf{W}'_d \mathbf{G}_{(d)}$  is a bit more tricky to deal with, but algorithms for efficient computation have been developed, see Phan et al. (2013). The parameter  $\rho$  is user specified and can generally be set as any positive real number. Following the suggestion of Huang et al. (2016), we found success setting  $\rho = \mathbf{W}'_{D+1} \mathbf{W}_{D+1} / K$ .

---

**Algorithm 1** Algorithm to approximate the solution to (16)

---

- 1: **Input**  $\widehat{\mathcal{G}}, \{\mathbf{T}_d\}, \{\lambda_d\}$
  - 2: **Output**  $\tilde{\mathbf{C}}_1, \dots, \tilde{\mathbf{C}}_D, \mathbf{B}$
  - 3: **Initialize** For  $d = 1, \dots, D$ :  $\tilde{\mathbf{C}}_d; \mathbf{U}^*$  as zero matrices;  $\mathbf{B}$
  - 4: **while** change in  $\tilde{\mathbf{C}}_1, \dots, \tilde{\mathbf{C}}_D, \mathbf{B}$  is non-negligible **do**
  - 5:     **for**  $d = 1, \dots, D$  **do**
  - 6:         Update  $\tilde{\mathbf{C}}_d$  according to (18), by way of (20)
  - 7:     **while**  $r_{\text{primal}} > \text{tol}_{\text{primal}}$  or  $r_{\text{dual}} > \text{tol}_{\text{dual}}$  **do**
  - 8:         Update  $\mathbf{B}$  according to (22)
  - 9:         Update  $\mathbf{Z}$  according to (25)
  - 10:         Update  $\mathbf{U}^*$  according to (24)
  - 11:         Update  $r_{\text{primal}}, r_{\text{dual}}$  according to (26)
- 

### 3 Multidimensional Penalized FPCA

In Section 2, we argued that the  $K$ -oMPB is an appealing option for modeling multidimensional functional data, both due to attractive theoretical properties and the existence of efficient numerical algorithms to form estimates in practice. That said, the efficiency of the approximation performance, provided in Theorem 2.2, depends on the joint low-rank structure of the eigenfunctions of  $U$  under the chosen marginal basis system. For many real world datasets, it may be the case that the first  $K^* \ll K$  eigenfunctions can capture nearly the same proportion of variance of the data as the  $K$ -oMPB. Unfortunately, as was discussed in the introduction, the standard techniques for estimating the eigenfunctions (FPCA) suffer greatly from the curse of dimensionality. While  $K$ -oMPB may not be the optimal rank- $K$

basis system, with an appeal to the low-rank property observed in many real world datasets it is reasonable to assume that for *most*  $U$  there exists some  $K \ll m^D$ , for which  $\zeta^*$  captures nearly the same proportion of variance as  $\tau_m$ . Under this assumption, we can define a multidimensional FPCA using the *post-represented* data, i.e. the MPF representations of the sample  $\mathcal{Y}$  obtained from Algorithm 1, which avoids the curse of dimensionality while incurring only trivial additional computational expense. In the remainder of this section we outline the procedure for the proposed two-stage FPCA.

Consider the method for FPCA proposed by Silverman (1996), in which the  $j$ th eigenfunction  $\psi_j$  is defined as the function maximizing the penalized sample variance with modified orthogonality constraints

$$\begin{aligned} \hat{\psi}_j &= \max_{\psi \in \mathbb{W}^{\alpha,2}(\mathcal{M})} \frac{\sum_{i=1}^N \text{Var}(\langle \psi, u_i \rangle_{\mathcal{H}})}{\langle \psi, \psi \rangle_{\lambda}} \\ \text{s.t. } \quad &\|\psi\|_{\mathcal{H}}^2 = 1, \quad \langle \psi, \psi_k \rangle_{\lambda} = 0, \text{ for } k = 1, 2, \dots, j-1. \end{aligned} \quad (27)$$

Here  $\langle \psi, \psi_k \rangle_{\lambda} \equiv \langle \psi, \psi_k \rangle_{\mathcal{H}} + \lambda \langle L(\psi_j), L(\psi_k) \rangle_{\mathcal{H}}$  and  $L : \mathbb{W}^{\alpha,2}(\mathcal{M}) \rightarrow \mathcal{H}$  is an  $\alpha$ th order linear differential operator quantifying the global roughness. For simplicity, hereafter we define  $L := \Delta_{\mathcal{M}}$ , the Laplacian operator on  $\mathcal{M}$ , though other differential operators can be incorporated effortlessly. We choose a framework for FPCA that facilitates the optional incorporation of a flexible global roughness penalty in case a particular application requires a supplement to the marginally independent regularization imposed using penalties of the form in Assumption 2, e.g. penalizing mixed partial derivatives.

In the 1-dimensional case, the optimization problem (27) can be efficiently solved using a two-stage approach; first computing  $\hat{u}_i$  through expansion over some suitable basis system and then looking for solutions  $\hat{\psi}_j$  in the span of that set of basis functions. Analogously, we can first represent the realizations with the  $K$ -oMPB:  $\hat{u}_i(\mathbf{x}) = \mathbf{b}'_i \zeta^*(\mathbf{x})$ , and then solve Equation (27) with the additional constraint  $\hat{\psi}_j \in \text{span}(\zeta^*)$ , i.e. look for solutions  $\hat{\psi}_j(\mathbf{x}) = \sum_{k=1}^K s_{jk} \zeta_k^*(\mathbf{x})$  for some  $\mathbf{s}_j = (s_{j1}, \dots, s_{jK})' \in \mathbb{R}^K$ . Under this setup, the optimization problem (27) is equivalent to

$$\begin{aligned} \mathbf{s}_j &= \max_{\mathbf{s}} \frac{\mathbf{s}' \mathbf{J}_{\zeta^*} \Sigma_b \mathbf{J}_{\zeta^*} \mathbf{s}}{\mathbf{s}' \mathbf{J}_{\zeta^*} \mathbf{s} + \lambda \mathbf{s}' \mathbf{R}_{\zeta^*} \mathbf{s}} \\ \text{s.t. } \quad &\mathbf{s}' \mathbf{J}_{\zeta^*} \mathbf{s} = 1, \quad \mathbf{s}' [\mathbf{J}_{\zeta^*} + \lambda \mathbf{R}_{\zeta^*}] \mathbf{s}_k = 0, \text{ for } k = 1, 2, \dots, j-1. \end{aligned} \quad (28)$$

Here  $\Sigma_{\mathbf{b}} = \text{Cov}(\mathbf{b})$  and  $\mathbf{J}_{\zeta^*}$ ,  $\mathbf{R}_{\zeta^*}$  are symmetric PSD matrices with elements  $[\mathbf{J}_{\zeta^*}]_{ij} = \langle \zeta_i^*, \zeta_j^* \rangle_{\mathcal{H}}$  and  $[\mathbf{R}_{\zeta^*}]_{ij} = \langle \Delta_{\mathcal{M}}(\zeta_i^*), \Delta_{\mathcal{M}}(\zeta_j^*) \rangle_{\mathcal{H}}$ , respectively. The objective function in Equation (28) is a generalized Rayleigh quotient and it can be shown that the solutions for  $j = 1, \dots, K^*$  are equivalently defined by the first  $K^*$  solutions to the generalized eigenvalue problem

$$\mathbf{J}_{\zeta^*} \Sigma_{\mathbf{s}} \mathbf{J}_{\zeta^*} \mathbf{s}_j = \gamma_j [\mathbf{J}_{\zeta^*} + \lambda \mathbf{R}_{\zeta^*}] \mathbf{s}_j. \quad (29)$$

Therefore, the vector of estimated eigenfunctions is  $\hat{\boldsymbol{\psi}}(\mathbf{x}) := (\mathbf{s}'_1 \boldsymbol{\zeta}^*(\mathbf{x}), \dots, \mathbf{s}'_{K^*} \boldsymbol{\zeta}^*(\mathbf{x}))'$ .

Notably, due to the marginal product structure of  $\boldsymbol{\zeta}^*$ , the  $D$ -dimensional integrals and partial derivatives required for the computation of  $\mathbf{J}_{\zeta^*}$  and  $\mathbf{R}_{\zeta^*}$  decompose into simple sums and products of integrals and derivatives over the marginal spaces. This highlights an important practical advantage of working with the marginal product structure, as it allows us to circumvent the potentially enormous computational cost of performing numerical integration/differentiation of an arbitrary  $D$ -dimensional function. Of course,  $\boldsymbol{\zeta}^*$ , and hence  $\mathbf{J}_{\zeta^*}$ ,  $\mathbf{R}_{\zeta^*}$ , and  $\Sigma_{\mathbf{b}}$  are unknown and must be estimated from the data. For further discussion on these topics as well as pseudocode for the two stage regularized multidimensional FPCA, see Section S3 and Algorithm 2 in the Supplementary Text.

## 4 Simulation Study

### 4.1 Representing a Random Sample

In this section, we compare three methods for constructing the functional representation of a random sample generated from a marginal product functional model: 1) a tensor product basis system estimated by the sandwich smoother (Xiao et al., 2013), 2) the FCP-TPA algorithm (Allen, 2013), and 3) the  $K$ -oMPB estimated using Algorithm 1, referred to in this section as **MARGARITA** (**M**ARGinal-product **b**asis **R**epresentation **w**ith **T**ensor **A**nalysis). A brief overview of the two competing methods is provided in Section S5, Supplementary Text.

The random function in our simulation is defined by the marginal product form;

$$U(\mathbf{x}) = \sum_{k=1}^{K^t} A_k^t \prod_{d=1}^D (\mathbf{c}_{d,k}^t)' \phi_j^t(x_d).$$

Here  $\phi_j^t$  is the period-1 Fourier basis expansion, i.e. for  $n \in \mathbb{N}$

$$\phi_{j,0}^t = \frac{1}{\sqrt{2}}, \quad \phi_{j,2n-1}^t = \sin(2\pi n x_j), \quad \phi_{j,n}^t = \cos(2\pi n x_j).$$

$\mathbf{c}_{d,k}^t$  is the  $k$ th column vector of  $\mathbf{C}_d^t$ , the fixed marginal factor matrix such that each element is an *i.i.d.* sample from  $\mathcal{N}(0, 0.3^2)$ ; and  $(A_1^t, \dots, A_K^t)' \sim \mathcal{N}(\mathbf{0}, \Sigma_A^t)$ . In other words,  $U$  is a mean-zero Gaussian random field. The covariance matrix is constructed as  $\Sigma_A^t = \mathbf{O}\mathbf{D}\mathbf{O}'$ , where  $\mathbf{O}$  is a random  $K^t \times K^t$  orthogonal matrix (sampled according to the Haar measure on  $\mathcal{O}(K^t)$ ), and  $\mathbf{D}$  is a diagonal matrix with  $\mathbf{D}_{kk} = \exp(-0.7k)$  for  $k = 1, \dots, K^t$ , i.e. an exponential decay model of the spectrum. We took the function domain to be the unit cube  $\mathcal{M} = [0, 1]^3$ . We fixed the true marginal basis dimensions to be  $m_d^t = 11$  for all  $d$  and considered true ranks  $K_t = 10$  and  $20$ .

For both ranks, all combinations of the following sampling settings are considered. High vs low SNR; obtained by taking of  $\sigma^2$  to be 0.5 and 10, small vs. large domain sample size;  $n_d = 30$  or 50 for all  $d$ , respectively, and small vs. large subject sample size; where  $N$  is taken to be 5 or 50, respectively. For each of these settings, 100 replications are simulated according to Model (13). The performance of the fitting methods are assessed by computing the mean integrated squared error (MISE) for each replication. That is, for each replication  $r$ , an estimate of the MISE is

$$\text{MISE}^{(r)} = \sum_{i=1}^{N^{(r)}} \int_{[0,1]^3} \left[ u_i^{(r)}(\mathbf{x}) - \hat{u}_i^{(r)}(\mathbf{x}) \right]^2 d\mathbf{x},$$

where  $\hat{u}_i^{(r)}$  is an estimate of  $u_i^{(r)}$  from the  $r$ th simulated dataset. Denote the Monte Carlo average of the MISE as  $\text{moMISE} = 100^{-1} \sum_{r=1}^{100} \text{MISE}^{(r)}$ .

We believe a fair comparison between the tensor product basis and MARGARITA should be based on enforcing (roughly) equivalently sized parameter spaces, i.e. total number of degrees of freedom. The total number of model parameters for the tensor product basis and MARGARITA are given by  $\prod_{d=1}^D m_d$  and  $K_{\text{fit}} \sum_{d=1}^D m_d$ , respectively. For the latter, we considered  $K_{\text{fit}} = 8, 15$ , or  $25$  and use a marginal cubic B-spline basis of rank 15 or 25. The second order derivative was used to define the marginal roughness penalties and a ridge penalty was used for regularization on the coefficients. For the former we use a tensor product of marginal cubic B-splines with marginal rank set equal to the smallest integer  $m_d$

such that  $m_d^3 \geq K_{\text{fit}} \sum_{d=1}^D m_d$ . For both FCP-TPA and **MARGARITA**, the penalty parameters were chosen through a grid search. For the tensor product basis, the smoothing parameters were selected by minimizing the GCV criterion from Xiao et al. (2013), implemented via the `enhance()` function from R package `hero` (French, 2020). All simulations were performed on a machine equipped with a 2.4 GHz Intel Xeon CPU E5-2695 and 24GB of RAM.

For all combinations of rank and sampling plans considered, the **MARGARITA** fits had substantially lower moMISE compared to the tensor product basis fits with comparable degrees of freedom. This is highlighted in Figure 1, which shows a comparison of the fit performance of the sandwich smoother and **MARGARITA** as a function of model degrees of freedom, for a subset of the simulation settings considered. Further discussion of these results as well as a tabular display of the moMISE for each simulation setting and model parameterization, are provided in Section S5 and Table S1 in the Supplementary Text. For the remainder of this section, we focus on comparing FCP-TPA and **MARGARITA**.

Figure 2 shows boxplots of the MISE for FCP-TPA and **MARGARITA** for each combination of marginal and global ranks,  $m_d$  and  $K_{\text{fit}}$  respectively, for several combinations of sample size  $N$  and marginal domain size  $n_d$ . For all panels,  $K_t = 20$  and  $\sigma^2 = 10$ . For all combinations of state of nature and model parameters considered, **MARGARITA** results in fits with lower moMISE than FCP-TPA. The separation in performance is more apparent in models with larger rank. An exhaustive tabular comparison of the moMISE for FCP-TPA and **MARGARITA** for all simulation settings considered is provided in Table S2 of Section S5, Supplementary Text. It leads to similar conclusions as the results presented in Figure 2.

We also compared the computational time of FCP-TPA and **MARGARITA** for each of the simulated datasets. For the small sample size, small sample domain case, the computational speed is comparable between the two algorithms. As both  $N$  and  $n_d$  increase, **MARGARITA** begins to comparatively fare better, culminating in significantly faster performance in the  $N = 50$ ,  $n_d = 50$  case. These results are shown in Figure S1, Supplementary Text. This trend is expected, since increasing  $n_d$  does not increase the dimension of the optimization problem (16) at the heart of Algorithm 1. On the other hand, the factors estimated with FCP-TPA are of dimension  $n_d$ , and thus the computational performance of the method can be expected to degrade as  $n_d$  increases. This highlights the practical importance of our

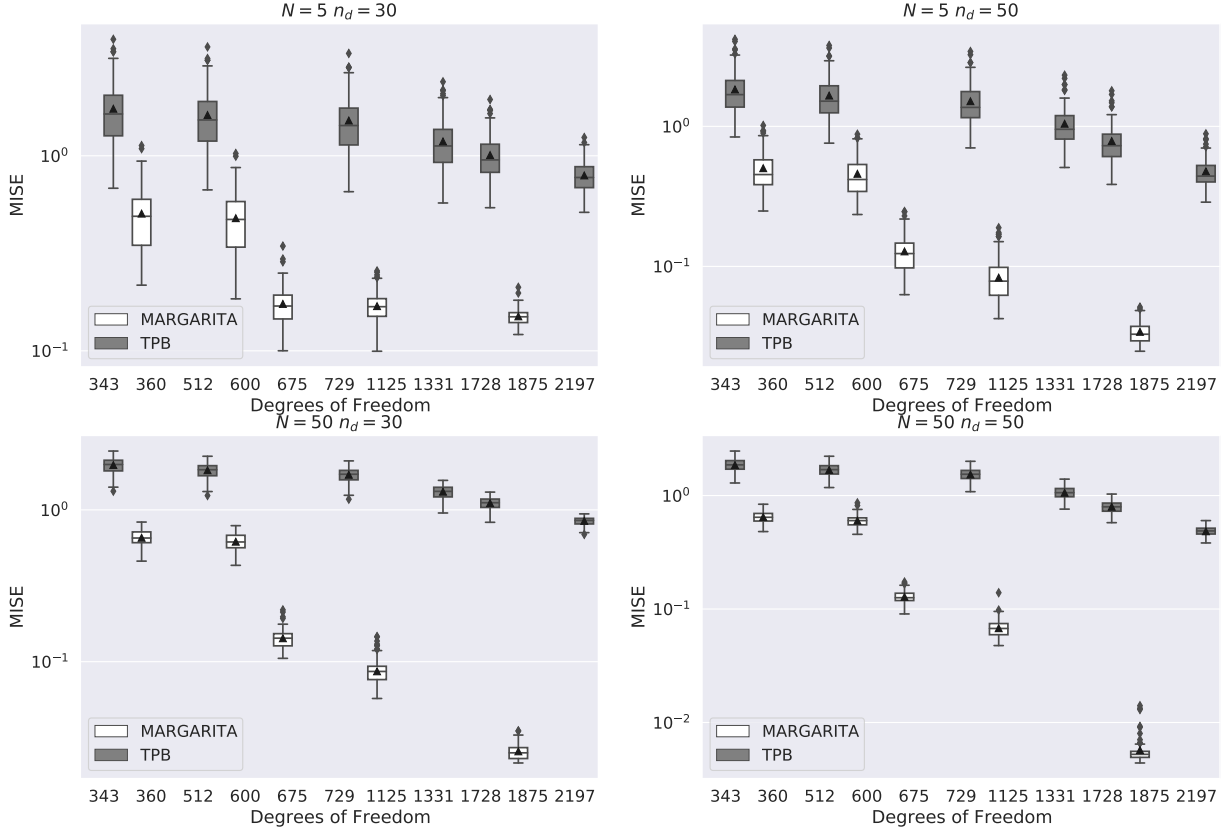


**Figure 1:** Comparison of the fit performance measured by MISE between the tensor product basis estimated by the sandwich smoother (gray) and MARGARITA (white) as a function of the total number of degrees of freedom. For each panel  $K_t = 20$  and  $\sigma^2 = 10$ , but similar patterns emerge for the  $K_t = 10$  and  $\sigma^2 = 0.5$  cases as well. The Y-axis is plotted on log-scale for clarity.

methods ability to control the dimension of the optimization problem.

## 4.2 Representing a New Realization

Let us assume that we have pre-trained  $\hat{\zeta}^*$  from a training data  $\mathcal{Y}$ , using MARGARITA. In this section, we would like to use  $\hat{\zeta}^*$  to construct a continuous representation of new data  $\mathbf{y}^\dagger \in \mathbb{R}^{n^\dagger}$ , by the standard least squares fitting principle, i.e. the estimator under which the optimality of  $\zeta^*$  is defined. Here  $\mathbf{y}^\dagger$  is the discrete data of a new realization  $u^\dagger \sim U$  observed at domain points  $\mathbf{X}^\dagger = (\mathbf{x}_1^\dagger, \dots, \mathbf{x}_{n^\dagger}^\dagger)'$ . Note that  $\mathbf{X}^\dagger$  could correspond to a flattened version of the grid  $\mathcal{X}$ , in which case  $\mathbf{y}^\dagger$  is observed at the same set of locations as  $\mathcal{Y}$ , but this need not be the case.

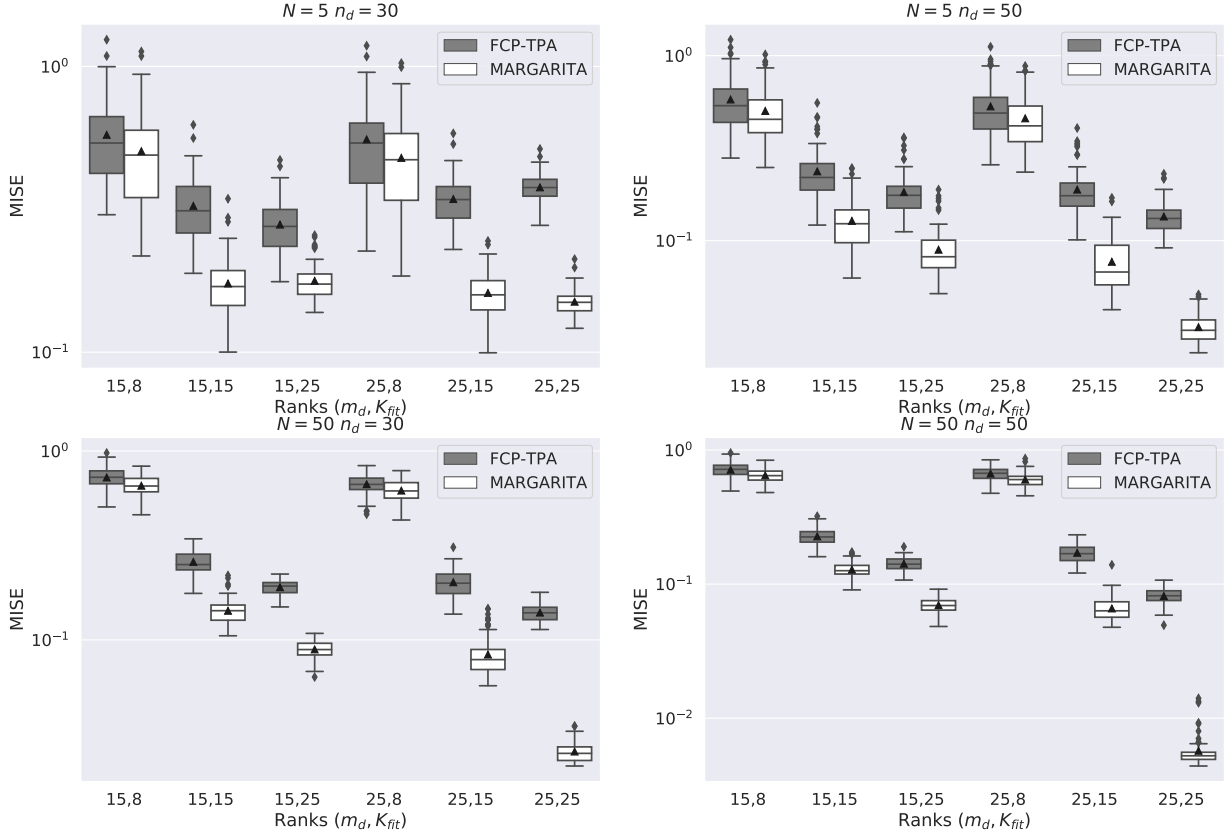


**Figure 2:** MISE of marginal product fits resulting from both FCP-TPA (gray) and MARGARITA (white). moMISE is denoted by a triangle. The Y-axis is plotted on log-scale for clarity.

To evaluate the effectiveness of using a pre-trained MPB to represent new realizations, we perform a simulation study using the same data generating procedure described in Section 4.1 with a fixed domain size of  $n_d = 30$  and measurement error variance  $\sigma^2 = 10$ . 100 Monte Carlo datasets are simulated for a sequence of increasing training sample sizes ranging from  $N = 5$  to 200. Three separate basis systems are considered;  $K$ -oMPB basis with ranks 10 and 3, denoted  $\zeta_{(10)}^*$  and  $\zeta_{(3)}^*$ , estimated by applying MARGARITA to the training data, and the top 3 eigenfunctions estimated by applying the two-stage FPCA outlined in Section 3 using  $\zeta_{(10)}^*$ , denoted  $\psi_{(3)}$ . The dimension of the marginal basis system is fixed at  $m_d = 15$ . For each training set, continuous representations for each of 20 discrete realizations in an independent test set are estimated through least squares basis expansion over  $\zeta_{(10)}^*$ ,  $\zeta_{(3)}^*$  and  $\psi_{(3)}$ .

Table 1 compares the moMISE over the test set for each of the three basis systems.

Both  $\zeta_{(10)}^*$  and  $\psi_{(3)}$  show substantial improvement in test set performance as training size  $N$  increases. Alternatively, the moMISE of  $\zeta_{(3)}^*$  stays relatively constant over  $N$ , indicating the rank of the basis is not large enough to adequately model the signal in the training data. Comparing the performance of the two rank 3 basis systems,  $\zeta_{(3)}^*$  and  $\psi_{(3)}$ , it is clear that the two-stage FPCA procedure results in a far more expressive basis system than simply estimating fewer factors.

To contextualize the results, consider that under identical simulation conditions, it was observed that a tensor product basis system with 2,197 basis functions had a moMISE of about 0.8 (see Section S5 in Supplementary Text). Compare this with the proposed procedure, for which a set of basis functions are learned by incorporating sufficient prior information, say 200 training examples. The resulting rank-3 system,  $\psi_{(3)}$ , produces a lower moMISE ( $\approx 0.57$ ) while also constituting an enormous decrease in model complexity. Furthermore, the computational expenditure of representing new data with a pre-trained basis system is trivial for even moderately large  $K^*$ , as it is a simple linear least squares problem for which many fast and stable algorithms exist. For example, it took an average of  $\approx 0.92$  seconds to run MARGARITA on a set of  $N = 50$  samples with  $K = m_d = 25$ . If the  $K$ -oMPB is provided by pre-training, it took only on average  $\approx 0.0030$  seconds to represent the same data as smooth multi-dimensional functions, around a  $300\times$  savings. In other words, given *a priori* access to relevant historical data, we can learn a parsimonious basis system for representation of new data which does not suffer from the curse of dimensionality and thus can be used to facilitate downstream analysis tasks of interest.

## 5 Real Data Analysis

Diffusion tensor imaging (DTI) is a technique in diffusion weighted MRI which fits a  $3 \times 3$  covariance matrix (the diffusion tensor) at each voxel in the brain to model the direction of local water molecule diffusion (Basser et al., 1994). It is often of interest to quantify the anisotropy of the local diffusion, as high degrees of anisotropy generally indicate the presence of white matter (WM) fiber tracts which are useful for identifying the fine physical structure of the brain. Fractional anisotropy (FA) is a scalar measure of anisotropy that is computed

**Table 1:** Monte Carlo average of the MISE over the test set for each of the three pre-trained basis systems.  $\zeta_{(10)}^*$  and  $\zeta_{(3)}^*$  were obtained by applying MARGARITA to an independent training set with  $K = 10, 3$ , respectively.  $\psi_{(3)}$  was constructed from the first 3 eigenfunctions estimated using the two-stage FPCA procedure under basis  $\zeta_{(10)}^*$ .  $N$  indicates the number of training samples used to estimate the basis systems. Standard errors are given in parenthesis.

N	5	10	20	50	100	200
$\zeta_{(10)}^*$	0.620 (0.036)	0.529 (0.035)	0.528 (0.025)	0.493 (0.021)	0.492 (0.014)	0.454 (0.024)
$\zeta_{(3)}^*$	2.198 (0.098)	2.075 (0.123)	2.201 (0.110)	2.182 (0.107)	2.068 (0.072)	2.066 (0.114)
$\psi_{(3)}$	0.981 (0.066)	0.732 (0.039)	0.663 (0.029)	0.645 (0.027)	0.619 (0.017)	0.574 (0.030)

from the eigenvalues of the diffusion tensor and is widely used to analyze diffusion weighted images. Previous studies have shown the potential for using dMRI/DTI based analysis to identify white matter abnormalities associated with traumatic brain injury (TBI) and post concussive syndrome (Inglese et al., 2005; Kraus et al., 2007).

For this application, we leverage the proposed methodology to analyze the diffusion profiles of 50 subjects in an age matched balanced case-control TBI study. A diffusion tensor model is fit to each subject’s diffusion data and used to compute the per-voxel FA. Registration of the FA images to the ICBM 2009c Nonlinear Symmetric 1mm template (Fonov et al., 2009) is then performed using the popular ANTS software (Avants et al., 2009). The domain of analysis is constrained to be the convex hull of a rectangular  $115 \times 140 \times 120$  voxel grid in the template space covering the white matter, i.e. the raw data tensor  $\mathcal{Y} \in \mathbb{R}^{115 \times 140 \times 120 \times 50}$ . A white matter mask is also applied to the aligned data.

We compute a point-wise estimate of the mean function at each voxel by taking the mean of  $\mathcal{Y}$  along mode 4, which is then used to center the data. Note we could have used a variety of function approximation tools to estimate the mean, as this is a standard nonparametric regression task for an unknown deterministic multidimensional function, for example, a separate MPB for the mean (see Section S5.5, Supplementary Material). That said, we find that the raw empirical point-wise mean is sufficient for our aims. Cubic B-splines of ranks  $m_1 = 100, m_2 = 120, m_3 = 100$  are used as marginal basis systems and

the marginal roughness operator  $L_d$  is taken to be the second order derivative. A  $K$ -oMPB of rank  $K = 330$  is fit to the mean centered data tensor using MARGARITA. The penalty parameters are selected using a grid search while the marginal and global ranks are selected by sequentially training larger models until more than 85% of the variance in the raw data is captured. The multidimensional FPCA described in Section 3 is performed. The first  $K^* = 45$  eigenfunctions, which explain  $\approx 99\%$  of the represented variance, are used to model the data. All subsequent analysis is performed with respect to these eigenfunctions, denoted again as  $\psi$ .

We are interested in evaluating the capability of the learned functional representations to facilitate efficient downstream statistical analysis. To this end, we use the representations to formulate a prediction task to discriminate between control and TBI subjects. Specifically, a lasso penalized logistic regression classifier is trained to predict disease status using the subject coefficient vectors obtained by their representation over  $\psi$ . The resulting classification performance is evaluated using leave-one-out cross validation. Note that in order to prevent biasing of the results and to more faithfully simulate the clinical setting, the left-out subject is not included in the estimation of the  $K$ -oMPB. In order to obtain the coefficient vector for the left-out subject, a least squares estimator is used to project the raw-FA data into the span of  $\psi$ . The cross validated accuracy, precision and recall are approximately 0.88, 0.85, and 0.92, respectively, indicating substantial discriminatory power of the learned basis functions. These results are especially notable with the context that many voxel-based analysis of FA in TBI studies are not able to establish a significant group differences (Khong et al., 2016). Figure 3 shows a pair plot of the coefficients associated with 3 most informative eigenfunctions, as measured by the magnitude of the associated regression coefficient in the logistic classifier, for one of the predictive models trained during cross validation. Notice that there exists a substantial degree of separation for several of the bivariate plots. Figure 4 displays two cross sections of the template space. The blue, red and green areas indicate data driven regions of interest (ROIs), defined as areas where the values of the 3 most informative eigenfunctions are “extreme”, i.e. outside the 0.5% and 99.5% quantiles. The red and green ROIs in Figure 4(a) are within areas of the middle cerebellar peduncle (MCP), a structure composed of multiple fibers mostly involved in motor processing (Morales and

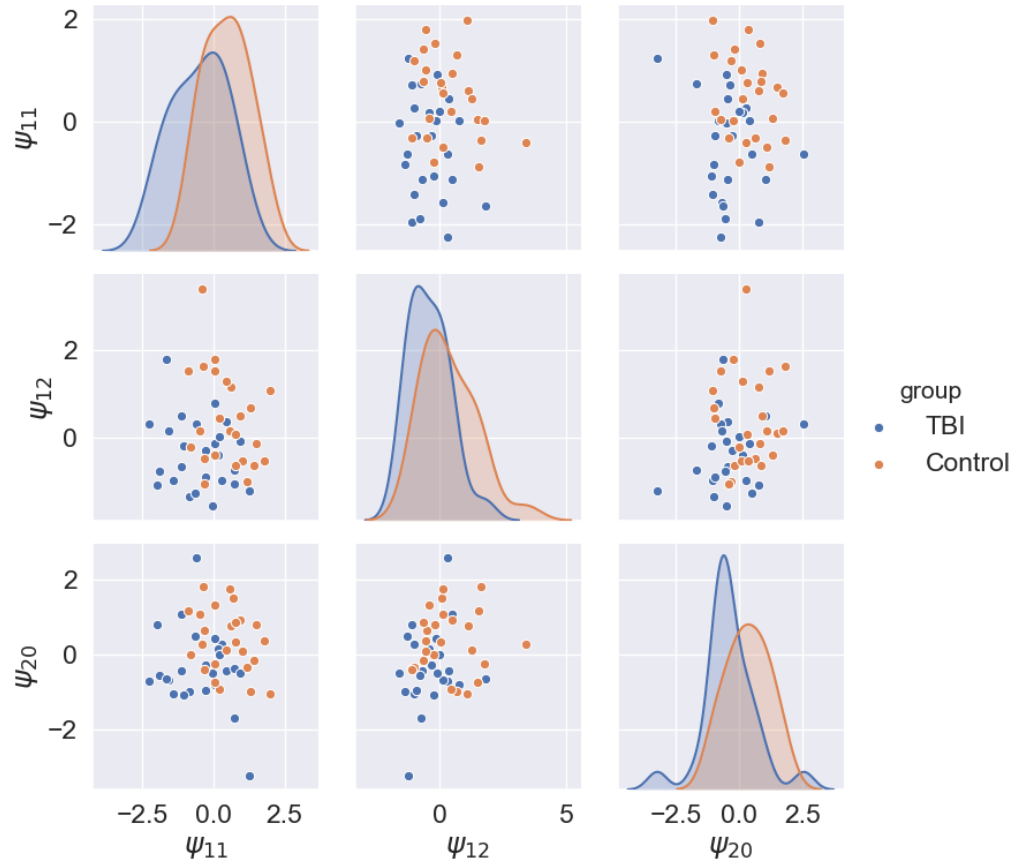
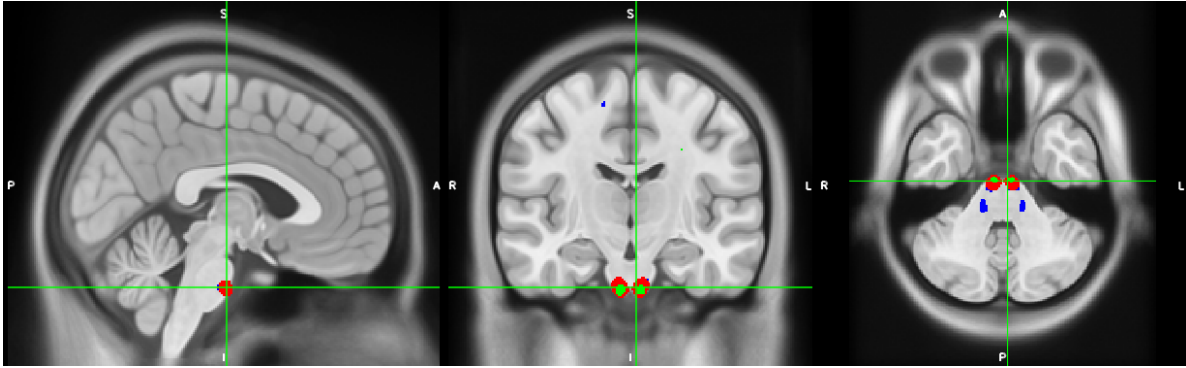
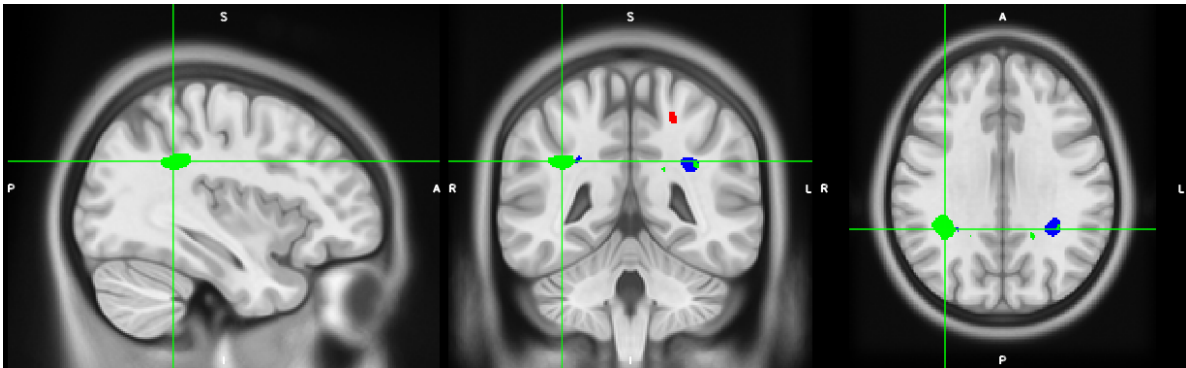


**Figure 3:** Pairwise scatter plots of the coefficients associated with the top 3 most important eigenfunctions, as determined by the logistic model. The panels along the diagonal show KDE for the marginal distributions. Each multidimensional eigenfunction provides some discriminatory power, as shown in the separation in the biplots. The logistic model trained on the full set of eigenfunction coefficients is able to distinguish TBI subjects from control with nearly 90% cross validated accuracy.

Tomsick, 2015). The green and blue ROIs in Figure 4(b) are within areas along the superior longitudinal fasciculus (SLF), a fiber bundle that is involved in higher-order motor and language processing (Petrides and Pandya, 2002). These areas are known to be affected in TBI (Wang et al., 2016; Xiong et al., 2014). For further discussion of these results and information on the study design and MRI scanning protocol, visit Section S6 in the Supplementary Material.



(a)



(b)

**Figure 4:** Data-driven ROIs created from thresholding the 0.5% and 99.5% quantiles of three most informative eigenfunctions, blue, red, and green, respectively. ROIs in plot (a) are within areas of the middle cerebellar peduncle and in plot (b) are in areas along the superior longitudinal fasciculus, both of which are known to be affected in TBI.

## 6 Discussion and Future Work

This work introduces a methodological framework and accompanying estimation algorithm for constructing an optimal and efficient continuous representation of multidimensional functional data. We consider basis functions that exhibit a marginal product structure and prove that an optimal set of such functions can be defined by the penalized tensor decomposition of an appropriate transformation of the raw data tensor. A separable roughness penalty is defined which can incorporate a variety of marginal differential regularizations to promote smoothness. Estimation of the model parameters is performed using a block coordinate descent scheme and we describe globally convergent numerical algorithms for

solving the subproblems. We further show how our method can be used to design an efficient approximation procedure for multidimensional FPCA. Using extensive simulation studies, we illustrate the superiority of our proposed method compared to alternative multidimensional function approximation schemes. In a real data application of the group-wise analysis of diffusion MRI, we show that our method can facilitate multidimensional functional data analysis tasks such as prediction and spatial region of interest identification.

One of the key ways the proposed method differs from alternative multidimensional tensor smoothing methodologies is the explicit estimation of a continuous set of basis functions. This continuous representation of the data permits the computationally efficient definition of operations such as inner products and partial derivatives, from which more complex operations can be built, e.g. functional regression, clustering, partial differential equation modeling. In the big data era, it is increasingly the case that large collections of publicly available historically relevant data can be acquired for many applications of interest, e.g. Human Connectome Project for brain MRI (Glasser et al., 2016). It is our vision that the proposed methodology can be applied to such historical databases and the learned basis systems saved and ported directly to subsequent analysis of data hypothesized to come from the same population. This pipeline will dramatically reduce both the computation requirements and the dimensionalities of the resulting models. Recall that the discrete diffusion data in Section 5 contained roughly 1.9 million voxels. Through the application of our methods we mapped the description of the data down to a dimension of 45, an approximately 40,000 times reduction, while still retaining enough signal to be able to predict disease status with high accuracy.

A major advantage of the proposed method is its computational efficiency, as discussed in Section 4 and further illustrated in Figure S1 of the Supplementary Text. The coordinate transformation at the heart of Theorem 2.4 allows the user to control the marginal dimension of the optimization problem. Simulation results recorded in Section S5 of the Supplementary Material indicate large saving in computational time compared to a tensor decomposition of the raw data, for moderately large grids. Another benefit of the proposed method is its modular structure. The marginal basis system, differential regularization and coefficient penalty function are all relatively generic, which allows for a variety of different specifications

that can be customized to the problem at hand. We implement our methods in a Python package named `eMFDA`, which is available at <https://github.com/Will-Consagra/eMFDA>. Our software is built for easy interface with the `scikit-fda` package: <https://github.com/GAA-UAM/scikit-fda>, and hence can take advantage of the large class of differential penalties and basis systems implemented therein.

We now discuss a couple issues and limitations of our methodology and suggest practical ways of circumventing them. First, in the statistical model for the observed data (13), we assume that the functional samples are observed on a common grid. In practice, this assumption may be overly restrictive: data may not be available at a subset of grid points for some samples, i.e. missing data. If the missingness rate is not too high, we could augment the loss function in Equation (16) to accommodate these missing values. This would clearly change the form of the updates (18) and (19), but algorithms have been proposed for solving similar problems (Huang et al., 2016). On the computational side, our method requires the specification of  $D + 1$  penalty parameters. In both simulation and real data experiments, we have found that performing cross validation over a grid of values centered at  $\|\mathbf{W}'_d \mathbf{W}_d\|_F / \|\mathbf{T}_d\|_F$  is typically sufficient for selecting a “good” penalty strength.

This work can be extended in several interesting directions. Right now, we are only considering least-squares based loss functions. One possible direction would be to extend this framework to more general loss functions, e.g. likelihood estimation with random functional parameters. As discussed, the penalty parameter selection is currently being performed through a grid search and therefore a principled derivation of a generalized cross validation criteria for our method is of interest. Up to this point, we have considered the  $\phi_d$ 's as fixed user-supplied parameters. In some cases, problem-specific prior information can be used to guide the selection of the marginal basis systems, e.g. Fourier basis if  $\mathcal{M}_d = \mathbb{S}^1$ . Additionally, if the number of marginal grid points  $n_d$  is not too large, using a locally supported basis, e.g. splines, with  $m_d = n_d$  and then promoting smoothness through selecting  $\lambda_d$  can be a good strategy. That said, we are often interested in the case when  $n_d$  is large and or  $\mathcal{M}_d$  is not an interval. In these more complicated situations, it is likely the case that optimizing over the marginal basis systems would result in substantially better performance of the resulting  $K$ -oMPB. We discuss one possible approach for augmenting the proposed methodology to

permit data-adaptive marginal basis systems in Section S4, Supplementary Text, but more work is needed. From a theoretical perspective, asymptotic analysis of the proposed method on a fixed grid can be performed using the theory of M-estimators, as was done in Zhou et al. (2013). If the grid is allowed to become arbitrarily fine, asymptotic analysis for this situation is non-trivial and would be an interesting direction of future research. Finally, for many applications it may be of interest to use external covariates to guide the construction of the optimal functional basis. This can be readily incorporated into the current framework by defining a two-stage functional canonical correlation analysis, analogous to the two-stage FPCA procedure from Section 3. That said, a single stage procedure may be preferable and would be an interesting direction of future inquiry.

## References

- Allen, G. I. (2013). Multi-way functional principal components analysis. In *2013 5th IEEE International Workshop on Computational Advances in Multi-Sensor Adaptive Processing (CAMSAP)*, pages 220–223.
- Allen, G. I. and Weylandt, M. (2019). Sparse and functional principal components analysis. *2019 IEEE Data Science Workshop (DSW)*.
- Avants, B. B., Tustison, N., and Song, G. (2009). Advanced normalization tools (ants). *Insight j*, 2(365):1–35.
- Barron, A. R., Cohen, A., Dahmen, W., and DeVore, R. A. (2008). Approximation and learning by greedy algorithms. *The Annals of Statistics*, 36(1):64 – 94.
- Bartels, R. H. and Stewart, G. W. (1972). Solution of the matrix equation  $ax + xb = c$  [f4]. *Commun. ACM*, 15(9):820–826.
- Basser, P. J., Mattiello, J., and LeBihan, D. (1994). MR diffusion tensor spectroscopy and imaging. *Biophysical Journal*, 66(1):259–267.
- Battaglino, C., Ballard, G., and Kolda, T. G. (2018). A practical randomized cp tensor decomposition. *SIAM Journal on Matrix Analysis and Applications*, 39(2):876–901.

- Bertsekas, D. P. (1997). Nonlinear programming. *Journal of the Operational Research Society*, 48(3):334–334.
- Beylkin, G., Garcke, J., and Mohlenkamp, M. J. (2009). Multivariate regression and machine learning with sums of separable functions. *SIAM Journal on Scientific Computing*, 31(3):1840–1857.
- Boyd, S., Parikh, N., Chu, E., Peleato, B., and Eckstein, J. (2011). Distributed optimization and statistical learning via the alternating direction method of multipliers. *Found. Trends Mach. Learn.*, 3(1):1–122.
- Brandstack, N., Kurki, T., and Tenovuo, O. (2013). Quantitative diffusion-tensor tractography of long association tracts in patients with traumatic brain injury without associated findings at routine mr imaging. *Radiology*, 267(1):231–239.
- Chen, L.-H. and Jiang, C.-R. (2017). Multi-dimensional functional principal component analysis. *Statistics and Computing*, 27(5):1181–1192.
- Chevreuril, M., Lebrun, R., Nouy, A., and Rai, P. (2015). A least-squares method for sparse low rank approximation of multivariate functions. *SIAM/ASA Journal on Uncertainty Quantification*, 3(1):897–921.
- Erichson, N. B., Manohar, K., Brunton, S. L., and Kutz, J. N. (2020). Randomized CP tensor decomposition. *Machine Learning: Science and Technology*, 1(2):025012.
- Fonov, V., Evans, A., McKinstry, R., Almlí, C., and Collins, D. (2009). Unbiased nonlinear average age-appropriate brain templates from birth to adulthood. *NeuroImage*, 47(Supplement 1):S102.
- French, J. (2020). *hero: Spatio-Temporal (Hero) Sandwich Smoother*. R package version 0.4.7.
- French, J. P. and Kokoszka, P. S. (2021). A sandwich smoother for spatio-temporal functional data. *Spatial Statistics*, 42:100413. Towards Spatial Data Science.

- Glasser, M. F., Smith, S. M., Marcus, D. S., Andersson, J. L., Auerbach, E. J., Behrens, T. E., Coalson, T. S., Harms, M. P., Jenkinson, M., Moeller, S., Robinson, E. C., Sotiropoulos, S. N., Xu, J., Yacoub, E., Ugurbil, K., and Van Essen, D. C. (2016). The Human Connectome Project’s neuroimaging approach. *Nature Neuroscience*, 19(9):1175–1187.
- Golub, G., Nash, S., and Van Loan, C. (1979). A hessenberg-schur method for the problem  $ax + xb = c$ . *IEEE Transactions on Automatic Control*, 24(6):909–913.
- Gorodetsky, A. A., Karaman, S., and Marzouk, Y. M. (2015). A continuous analogue of the tensor-train decomposition.
- Grasedyck, L., Kressner, D., and Tobler, C. (2013). A literature survey of low-rank tensor approximation techniques. *GAMM-Mitteilungen*, 36(1):53–78.
- Halko, N., Martinsson, P. G., and Tropp, J. A. (2011). Finding structure with randomness: Probabilistic algorithms for constructing approximate matrix decompositions. *SIAM Review*, 53(2):217–288.
- Hillar, C. and Lim, L.-H. (2013). Most tensor problems are np-hard.
- Hsing, T. and Eubank, R. (2015). Theoretical foundations of functional data analysis, with an introduction to linear operators. volume 997. John Wiley & Sons.
- Huang, J. Z., Shen, H., and Buja, A. (2009). The analysis of two-way functional data using two-way regularized singular value decompositions. *Journal of the American Statistical Association*, 104(488):1609–1620.
- Huang, K., Sidiropoulos, N. D., and Liavas, A. P. (2016). A flexible and efficient algorithmic framework for constrained matrix and tensor factorization. *IEEE Transactions on Signal Processing*, 64(19):5052–5065.
- Inglese, M., Makani, S., Johnson, G., Cohen, B. A., Silver, J. A., Gonen, O., and Grossman, R. I. (01 Jan. 2005). Diffuse axonal injury in mild traumatic brain injury: a diffusion tensor imaging study. *Journal of Neurosurgery*, 103(2):298 – 303.

- Kargas, N. and Sidiropoulos, N. D. (2021). Supervised learning and canonical decomposition of multivariate functions. *IEEE Transactions on Signal Processing*, 69:1097–1107.
- Khong, E., Odenwald, N., Hashim, E., and Cusimano, M. D. (2016). Diffusion tensor imaging findings in post-concussion syndrome patients after mild traumatic brain injury: A systematic review. *Frontiers in Neurology*, 7:156.
- Kolda, T. G. and Bader, B. W. (2009). Tensor decompositions and applications. *SIAM review*, 51(3):455–500.
- Kraus, M. F., Susmaras, T., Caughlin, B. P., Walker, C. J., Sweeney, J. A., and Little, D. M. (2007). White matter integrity and cognition in chronic traumatic brain injury: a diffusion tensor imaging study. *Brain*, 130(10):2508–2519.
- Li, N., Kindermann, S., and Navasca, C. (2013). Some convergence results on the regularized alternating least-squares method for tensor decomposition. *Linear Algebra and its Applications*, 438(2):796–812. Tensors and Multilinear Algebra.
- Li, Y., Huang, C., and Härdle, W. K. (2019). Spatial functional principal component analysis with applications to brain image data. *Journal of Multivariate Analysis*, 170:263 – 274. Special Issue on Functional Data Analysis and Related Topics.
- Morales, H. and Tomsick, T. (2015). Middle cerebellar peduncles: Magnetic resonance imaging and pathophysiologic correlate. *World journal of radiology*, 7(12):438.
- Nouy, A. (2017). Low-rank tensor methods for model order reduction. *Handbook of Uncertainty Quantification*, page 857–882.
- Parikh, N. and Boyd, S. (2014). Proximal algorithms. *Found. Trends Optim.*, 1(3):127–239.
- Petrides, M. and Pandya, D. N. (2002). Association pathways of the prefrontal cortex and functional observations. *Principles of frontal lobe function*, 1:31–50.
- Phan, A., Tichavský, P., and Cichocki, A. (2013). Fast alternating ls algorithms for high order candecomp/parafac tensor factorizations. *IEEE Transactions on Signal Processing*, 61(19):4834–4846.

- Post, A., Oeur, A., Hoshizaki, B., and Gilchrist, M. D. (2013). Examination of the relationship between peak linear and angular accelerations to brain deformation metrics in hockey helmet impacts. *Computer methods in biomechanics and biomedical engineering*, 16(5):511–519.
- Ramsay, J. (2005). *Functional Data Analysis*. American Cancer Society.
- Razaviyayn, M., Hong, M., and Luo, Z.-Q. (2013). A unified convergence analysis of block successive minimization methods for nonsmooth optimization. *SIAM Journal on Optimization*, 23(2):1126–1153.
- Ruppert, D., Wand, M., and Carroll, R. (2006). *Semiparametric Regression*, volume 101.
- Silverman, B. W. (1996). Smoothed functional principal components analysis by choice of norm. *Ann. Statist.*, 24(1):1–24.
- Stone, C. J. (1980). Optimal rates of convergence for nonparametric estimators. *The Annals of Statistics*, 8(6):1348–1360.
- Suzuki, T., Kanagawa, H., Kobayashi, H., Shimizu, N., and Tagami, Y. (2016). Minimax optimal alternating minimization for kernel nonparametric tensor learning. In Lee, D., Sugiyama, M., Luxburg, U., Guyon, I., and Garnett, R., editors, *Advances in Neural Information Processing Systems*, volume 29. Curran Associates, Inc.
- Temlyakov (2003). Nonlinear methods of approximation. *Foundations of Computational Mathematics*, 3(1):33–107.
- Wang, J., Wong, R. K. W., and Zhang, X. (2020). Low-rank covariance function estimation for multidimensional functional data.
- Wang, Z., Wu, W., Liu, Y., Wang, T., Chen, X., Zhang, J., Zhou, G., and Chen, R. (2016). Altered cerebellar white matter integrity in patients with mild traumatic brain injury in the acute stage. *PLoS One*, 11(3):e0151489.
- Wasserman, L. (2010). *All of Nonparametric Statistics*. Springer Publishing Company, Incorporated, 1st edition.

- Wood, S. N. (2011). Fast stable restricted maximum likelihood and marginal likelihood estimation of semiparametric generalized linear models. *Journal of the Royal Statistical Society (B)*, 73(1):3–36.
- Xiao, L., Li, Y., and Ruppert, D. (2013). Fast bivariate p-splines: the sandwich smoother. *Journal of the Royal Statistical Society: Series B (Statistical Methodology)*, 75(3):577–599.
- Xiong, K., Zhu, Y., Zhang, Y., Yin, Z., Zhang, J., Qiu, M., and Zhang, W. (2014). White matter integrity and cognition in mild traumatic brain injury following motor vehicle accident. *Brain research*, 1591:86–92.
- Yao, F., Müller, H.-G., and Wang, J.-L. (2005). Functional data analysis for sparse longitudinal data. *Journal of the American Statistical Association*, 100(470):577–590.
- Zhang, J.-T. and Chen, J. (2007). Statistical inferences for functional data. *The Annals of Statistics*, 35(3):1052 – 1079.
- Zhou, H., Li, L., and Zhu, H. (2013). Tensor regression with applications in neuroimaging data analysis. *Journal of the American Statistical Association*, 108(502):540–552. PMID: 24791032.

# Supplementary Text: Efficient Multidimensional Functional Data Analysis Using Marginal Product Basis Systems

William Consagra      Arun Venkataraman      Xing Qiu\*

**Remark:** Equations defined in this supplementary text are all labeled by “Equation (S<n>)” convention, so that they can be distinguished from those defined in the main text, which do not have prefix “S”.

## S1 Theory and Proofs

### S1.1 Proof of Propositions 2.1 and 2.6

#### Proof of propositions 2.1

*Proof.* To see that  $\text{span}(\zeta^*) = \mathcal{L}_{m,K}$ , note that this is true for any  $\zeta \in \mathcal{V}_{m,K}$  since there can be at most  $m^D$  linearly independent  $\zeta_k$ . To show  $\mathcal{L}_{m,K} = \mathcal{H}_m$ , first note that by definition,  $\mathcal{L}_{m,K} \subset \mathcal{H}_m$ . Furthermore, for any  $v \in \tau_m$ , we have  $v \in \mathcal{L}_m$ . Since  $K = m^D \equiv |\tau_m|$ , it follows that  $\mathcal{H}_m \subset \mathcal{L}_{m,K}$ . □

#### Proof of propositions 2.6

*Proof.* Denote the matrix  $\mathbf{R}_d(i, j) = \int_{\mathcal{M}_d} L_d(\phi_{d,i})L_d(\phi_{d,j})$ . Then we have

$$\begin{aligned} \int_{\mathcal{M}_d} L_d^2(\xi_{k,d}) &= \mathbf{c}'_{d,k} \mathbf{R}_d \mathbf{c}_{d,k} \\ &= \tilde{\mathbf{c}}'_{d,k} \mathbf{D}_d^{-1} \mathbf{V}'_d \mathbf{R}_d \mathbf{V}_d \mathbf{D}_d^{-1} \tilde{\mathbf{c}}_{d,k} \\ &\equiv \tilde{\mathbf{c}}'_{d,k} \mathbf{T}_d \tilde{\mathbf{c}}_{d,k}. \end{aligned}$$

The result follows by noting that  $\mathbf{T}_d$  is a symmetric product of positive semidefinite matrices and therefore is symmetric and positive semidefinite. □

## S1.2 Proof of Theorem 2.2

**Proposition S1.** *The coefficients of the oracle estimator  $u^*(\zeta)$  (9), for  $\zeta \in \mathcal{V}_{m,K}$  are given by*

$$\mathbf{b}^* := (b_1^*, \dots, b_K^*) = \sum_{l=1}^{\infty} Z_l \mathbf{b}_l^*$$

*Proof.* Follows trivially from the analytic definition of the least squares estimator coupled with the independence of the elements of the space  $\mathcal{V}_{m,K}$ .  $\square$

We now give a proof of Theorem 2.2.

*Proof.* Define  $\mathcal{H}_m^\perp$  as the orthogonal complement of  $\mathcal{H}_m$  in  $\mathcal{H}$  and denote  $P_{\mathcal{H}_m}$  and  $P_{\mathcal{H}_m^\perp}$  the corresponding projection operators. We have

$$\begin{aligned} \inf_{\zeta \in \mathcal{V}_{m,K}} \mathbb{E} \|U - u^*(\zeta)\|_{\mathcal{H}}^2 &= \inf_{\zeta \in \mathcal{V}_{m,K}} \mathbb{E} \|(P_{\mathcal{H}_m}(U) - u^*(\zeta)) + P_{\mathcal{H}_m^\perp}(U)\|_{\mathcal{H}}^2 \\ &= \inf_{\zeta \in \mathcal{V}_{m,K}} \mathbb{E} \|P_{\mathcal{H}_m}(U) - u^*(\zeta)\|_{\mathcal{H}_m}^2 \\ &\quad + 2\mathbb{E} \langle (P_{\mathcal{H}_m}(U) - u^*(\zeta)), P_{\mathcal{H}_m^\perp}(U) \rangle_{\mathcal{H}} \\ &\quad + \mathbb{E} \|P_{\mathcal{H}_m^\perp}(U)\|_{\mathcal{H}_m^\perp}^2 \\ &:= \text{Term}_1 + \text{Term}_2 + \text{Term}_3. \end{aligned}$$

Term<sub>3</sub> is independent of  $\zeta$  and represents the expected irreducible error due to the finite dimensional truncation of the marginal basis systems. We have

$$\begin{aligned} \text{Term}_3 &= \mathbb{E} \|P_{\mathcal{H}_m^\perp}(U)\|_{\mathcal{H}_m^\perp}^2 = \mathbb{E} \left\| \sum_{k=1}^{\infty} Z_k P_{\mathcal{H}_m^\perp}(\psi_k) \right\|_{\mathcal{H}_m^\perp}^2 \\ &= \sum_{k=1}^{\infty} \mathbb{E} [Z_k^2] \cdot \|P_{\mathcal{H}_m^\perp}(\psi_k)\|_{\mathcal{H}_m^\perp}^2 \\ &= O(w_{\tau_m}(m)), \end{aligned} \tag{S.1}$$

where the second line follows from the  $Z_k$  being uncorrelated and the third line follows since  $\sum_{k=1}^{\infty} \mathbb{E} [Z_k^2] = \sum_{k=1}^{\infty} \rho_k < \infty$ . Since  $u^*(\zeta) \in \mathcal{L}_{m,K} \subset \mathcal{H}_m$  with probability one (w.p.1.), it is easy to see that Term<sub>2</sub> = 0 and thus we need only to deal with Term<sub>1</sub>.

The mapping  $\iota : \mathcal{H}_m \rightarrow \bigotimes_{d=1}^D \mathbb{R}^m$  defined by  $\iota(u)_{j_1, \dots, j_D} = a_{j_1, \dots, j_D}$  is an isometry between inner product spaces  $(\mathcal{H}_m, \langle \cdot, \cdot \rangle_{\mathcal{H}_m})$  and  $(\bigotimes_{d=1}^D \mathbb{R}^m, \langle \cdot, \cdot \rangle_{\tilde{F}})$ , where  $a_{j_1, \dots, j_D}$  is the coefficient

of  $u$  associated with basis element  $\prod_{d=1}^D \phi_{d,j_d}$ . Recall from (7) that any  $u \in \mathcal{L}_{m,K}$  has the representation

$$u(\mathbf{x}) = \sum_{k=1}^K b_k \prod_{d=1}^D \sum_{j=1}^m c_{k,d,j} \phi_{d,j}(x_d)$$

and hence, under  $\iota$ , is identified with the tensor rank- $K$  tensor  $\sum_{k=1}^K b_k \otimes_{d=1}^D \mathbf{c}_{d,k}$ , where  $\mathbf{c}_{d,k}$  are the  $m$ -vectors of coefficients for the  $k$ th marginal function in the  $d$ th dimension. Since for any  $\zeta \in \mathcal{V}_{m,K}$ ,  $u^*(\zeta) \in \mathcal{L}_{m,K}$  w.p.1., it follows that

$$\begin{aligned} \|P_{\mathcal{H}_m}(U) - u^*(\zeta)\|_{\mathcal{H}_m}^2 &= \|P_{\mathcal{H}_m}(U) - u^*(\zeta)\|_{\mathcal{H}_m}^2 \\ &= \left\| \sum_{l=1}^{\infty} Z_l \mathcal{A}_l - \sum_{k=1}^K b_k^* \otimes_{d=1}^D \mathbf{c}_{d,k} \right\|_{\tilde{F}}^2. \end{aligned}$$

With slight abuse of notation,  $\iota(\mathcal{V}_{m,K}) = \mathcal{C}_{m,K}$ . Now, we have

$$\begin{aligned} \mathbb{E} \left\| \sum_{l=1}^{\infty} Z_l \mathcal{A}_l - \sum_{k=1}^K b_k^* \otimes_{d=1}^D \mathbf{c}_{d,k} \right\|_{\tilde{F}}^2 &= \mathbb{E} \left\| \sum_{l=1}^{\infty} Z_l \mathcal{A}_l - \sum_{k=1}^K b_k^* \otimes_{d=1}^D \mathbf{c}_{d,k} \right\|_{\tilde{F}}^2 \\ &= \mathbb{E} \left\| \sum_{l=1}^{\infty} Z_l \mathcal{A}_l - \sum_{k=1}^K \sum_{j=1}^{\infty} Z_l b_{j,k}^* \otimes_{d=1}^D \mathbf{c}_{d,k} \right\|_{\tilde{F}}^2 \\ &= \mathbb{E} \left\| \sum_{l=1}^{\infty} Z_l \mathcal{A}_l - \sum_{k=1}^K Z_l b_{l,k}^* \otimes_{d=1}^D \mathbf{c}_{d,k} \right\|_{\tilde{F}}^2 \\ &= \sum_{l=1}^{\infty} \mathbb{E}[Z_l^2] \left\| \mathcal{A}_l - \sum_{k=1}^K b_{l,k}^* \otimes_{d=1}^D \mathbf{c}_{d,k} \right\|_{\tilde{F}}^2 \\ &\quad + \sum_{j \neq r} \mathbb{E}[Z_j Z_r] \langle \mathcal{A}_j - \sum_{k=1}^K b_{j,k}^* \otimes_{d=1}^D \mathbf{c}_{d,k}, \mathcal{A}_r - \sum_{k=1}^K b_{r,k}^* \otimes_{d=1}^D \mathbf{c}_{d,k} \rangle_{\tilde{F}} \\ &= \sum_{l=1}^{\infty} \rho_l \left\| \mathcal{A}_l - \sum_{k=1}^K b_{l,k}^* \otimes_{d=1}^D \mathbf{c}_{d,k} \right\|_{\tilde{F}}^2 \\ &= \sum_{l=1}^K \rho_l \left\| \mathcal{A}_l - \sum_{k=1}^K b_{l,k}^* \otimes_{d=1}^D \mathbf{c}_{d,k} \right\|_{\tilde{F}}^2 + O(h(K)), \end{aligned}$$

where the second equality follows from proposition S1 and the fifth from  $\mathbb{E}[Z_k Z_j] = \rho_k \delta_{jk}$ , hence the desired result follows.  $\square$

### S1.3 Proof of Corollary 2.3

**Proposition S2.** Let  $P_{\mathcal{H}_{m,d}}$  be the projection operator for  $\mathcal{H}_{m,d}$  and denote

$$P_{\mathcal{H}_{m,d}}(\psi_{k,d}) = \prod_{d=1}^D \sum_{j=1}^m a_{d,k,j} \phi_{d,j}$$

for some set of coefficients  $\{a_{d,k,j}\}$ . Define the vector  $\mathbf{a}_{d,k} := (a_{d,k,1}, \dots, a_{d,k,m})' \in \mathbb{R}^m$ . Then

$$\mathcal{A}_k = \bigotimes_{d=1}^D \mathbf{a}_{d,k}$$

*Proof.* Follows directly from the separability assumption of the  $\psi_k$ 's.  $\square$

**Lemma S3.** Denote the matrix of marginal inner products

$$\mathbf{J}_{\zeta,m} = \begin{pmatrix} \prod_{d=1}^D \mathbf{a}'_{d,1} \mathbf{J}_{\phi_d} \mathbf{a}_{d,1} & \prod_{d=1}^D \mathbf{a}'_{d,1} \mathbf{J}_{\phi_d} \mathbf{a}_{d,2} & \cdots & \prod_{d=1}^D \mathbf{a}'_{d,1} \mathbf{J}_{\phi_d} \mathbf{a}_{d,K} \\ \prod_{d=1}^D \mathbf{a}'_{d,2} \mathbf{J}_{\phi_d} \mathbf{a}_{d,1} & \prod_{d=1}^D \mathbf{a}'_{d,2} \mathbf{J}_{\phi_d} \mathbf{a}_{d,2} & \cdots & \prod_{d=1}^D \mathbf{a}'_{d,2} \mathbf{J}_{\phi_d} \mathbf{a}_{d,K} \\ \vdots & \vdots & \ddots & \vdots \\ \prod_{d=1}^D \mathbf{a}'_{d,K} \mathbf{J}_{\phi_d} \mathbf{a}_{d,1} & \cdots & \cdots & \prod_{d=1}^D \mathbf{a}'_{d,K} \mathbf{J}_{\phi_d} \mathbf{a}_{d,K} \end{pmatrix},$$

Then we have the element-wise convergence rate

$$|\mathbf{J}_{\zeta,m}^{-1}(k, j) - \delta_{kj}| = O\left(\prod_{d=1}^D w_{\phi_d}(m)\right).$$

where  $w_{\phi_d}$  is the  $\mathbb{L}^2(\mathcal{M}_d)$  convergence rate of  $\phi_d$ , see Definition 2.3.

*Proof.* Consider that from the orthonormality of the  $\psi_k$ 's, we have the element-wise definition of the identity matrix

$$\begin{aligned} \mathbf{I}(k, j) &= \langle \psi_k, \psi_j \rangle_{\mathcal{H}} = \langle P_{\mathcal{H}_m}(\psi_k), P_{\mathcal{H}_m}(\psi_j) \rangle_{\mathcal{H}_m} + \langle P_{\mathcal{H}_m^\perp}(\psi_k), P_{\mathcal{H}_m^\perp}(\psi_j) \rangle_{\mathcal{H}_m^\perp} \\ &= \prod_{d=1}^D \mathbf{a}'_{d,k} \mathbf{J}_{\phi_d} \mathbf{a}_{d,j} + \prod_{d=1}^D \langle P_{\mathcal{H}_{m,d}^\perp}(\psi_{k,d}), P_{\mathcal{H}_{m,d}^\perp}(\psi_{j,d}) \rangle_{\mathcal{H}_{m,d}^\perp} \\ &= \mathbf{J}_{\zeta,m}(k, j) + \prod_{d=1}^D \langle P_{\mathcal{H}_{m,d}^\perp}(\psi_{k,d}), P_{\mathcal{H}_{m,d}^\perp}(\psi_{j,d}) \rangle_{\mathcal{H}_{m,d}^\perp} \end{aligned}$$

where the equality in the second line comes from the separability of the  $\psi_k$ 's. Therefore, we

have

$$\begin{aligned}
|\mathbf{J}_{\zeta,m}(k,j) - \mathbf{I}(k,j)| &= \left| \prod_{d=1}^D \langle P_{\mathcal{H}_{m,d}^\perp}(\psi_{k,d}), P_{\mathcal{H}_{m,d}^\perp}(\psi_{j,d}) \rangle_{\mathcal{H}_{m,d}^\perp} \right| \\
&\leq \prod_{d=1}^D \left\| P_{\mathcal{H}_{m,d}^\perp}(\psi_{k,d}) \right\|_{\mathcal{H}_{m,d}^\perp} \left\| P_{\mathcal{H}_{m,d}^\perp}(\psi_{j,d}) \right\|_{\mathcal{H}_{m,d}^\perp} \\
&= O\left( \prod_{d=1}^D w_{\phi_d}(m) \right).
\end{aligned}$$

Since the matrix inverse is Lipschitz continuous, it must be the case that  $|\mathbf{J}_{\zeta,m}^{-1}(k,j) - \mathbf{I}(k,j)| = O\left(\prod_{d=1}^D w_{\phi_d}(m)\right)$  and the desired result follows.  $\square$

**Lemma S4.** For any  $l, k \in \{1, \dots, K\}$ ,

$$|b_{l,k}^* - \delta_{lk}| = O\left(K \prod_{d=1}^D w_{\phi_d}(m)\right).$$

*Proof.* Define  $r_{m,l,k} = \langle P_{\mathcal{H}_m^\perp}(\psi_l), P_{\mathcal{H}_m^\perp}(\psi_k) \rangle_{\mathcal{H}_m^\perp} \equiv \prod_{d=1}^D \langle P_{\mathcal{H}_{m,d}^\perp}(\psi_{l,d}), P_{\mathcal{H}_{m,d}^\perp}(\psi_{k,d}) \rangle_{\mathcal{H}_{m,d}^\perp}$ . Notice that by Proposition S2 and the orthonormality of the eigenfunctions we have

$$\langle \mathcal{A}_l, \bigotimes_{d=1}^D \mathbf{a}_{d,k} \rangle_{\tilde{F}} = \begin{cases} 1 & k = l \\ -r_{l,m,k} & k \neq l \end{cases}.$$

Define the vector  $\mathbf{r}_{m,l} := (\mathbf{r}_{m,l,1}, \dots, \mathbf{r}_{m,l,l-1}, 0, \mathbf{r}_{m,l,l+1}, \dots, \mathbf{r}_{m,l,K})'$  and let  $\mathbf{e}_l$  be the  $l$ 'th unit vector, so  $\mathbf{b}_l^* = \mathbf{J}_{\zeta,m}^{-1}(\mathbf{e}_l - \mathbf{r}_{m,l})$ . We have

$$\begin{aligned}
|b_{l,k}^* - \delta_{lk}| &= \left| \sum_{j=1}^K \mathbf{J}_{\zeta,m}^{-1}(k,j) (\mathbf{e}_l(j) - \mathbf{r}_{m,l}(j)) - \delta_{lk} \right| \\
&= \left| \sum_{j=1}^K (\mathbf{J}_{\zeta,m}^{-1}(k,j) - \delta_{kj}) (\delta_{lj} - \mathbf{r}_{m,l}(j)) - \delta_{lk} \right| \\
&\leq \sum_{j=1}^K |(\mathbf{J}_{\zeta,m}^{-1}(k,j) - \delta_{kj}) (\delta_{lj} - \mathbf{r}_{m,l}(j))| + \sum_{j=1}^K |\delta_{kj} (\delta_{lj} - \mathbf{r}_{m,l}(j)) - \delta_{lk}| \\
&= \sum_{j=1}^K |(\mathbf{J}_{\zeta,m}^{-1}(k,j) - \delta_{kj})| |(\delta_{lj} - \mathbf{r}_{m,l}(j))| + |\mathbf{r}_{m,l}(k)| \\
&= O\left(\prod_{d=1}^D w_{\phi_d}(m)\right) \sum_{j=1}^K |(\delta_{lj} - \mathbf{r}_{m,l}(j))| + O\left(\prod_{d=1}^D w_{\phi_d}(m)\right) \\
&= O\left(\prod_{d=1}^D w_{\phi_d}(m)\right) \left(1 + \sum_{j \neq l} \mathbf{r}_{m,l}(j)\right) + O\left(\prod_{d=1}^D w_{\phi_d}(m)\right) \\
&= O\left(K \prod_{d=1}^D w_{\phi_d}(m)\right).
\end{aligned}$$

□

We are now ready to give a proof of Corollary 2.3.

*Proof.* We have

$$\begin{aligned}
\sum_{l=1}^K \rho_l \left\| \mathcal{A}_l - \sum_{k=1}^K b_{l,k}^* \bigotimes_{d=1}^D \mathbf{a}_{d,k} \right\|_{\tilde{F}}^2 &= \sum_{l=1}^K \rho_l \left\| \mathcal{A}_l - \sum_{k=1}^K \left( \delta_{lk} + O\left(K \prod_{d=1}^D w_{\phi_d}(m)\right) \right) \bigotimes_{d=1}^D \mathbf{a}_{d,k} \right\|_{\tilde{F}}^2 \\
&\leq \sum_{l=1}^K \rho_l \left[ \left\| \mathcal{A}_l - \bigotimes_{d=1}^D \mathbf{a}_{d,l} \right\|_{\tilde{F}}^2 + \sum_{k=1}^K O\left(K \prod_{d=1}^D w_{\phi_d}(m)\right) \left\| \bigotimes_{d=1}^D \mathbf{a}_{d,k} \right\|_{\tilde{F}}^2 \right] \\
&= O\left(K \prod_{d=1}^D w_{\phi_d}(m)\right) \sum_{l=1}^K \rho_l \sum_{k=1}^K \left\| \bigotimes_{d=1}^D \mathbf{a}_{d,k} \right\|_{\tilde{F}}^2 \\
&= O\left(K^2 \prod_{d=1}^D w_{\phi_d}(m)\right),
\end{aligned}$$

where the first equality comes from Lemma S4. This can be used to bound the first term on the RHS of Equation (11) in Theorem 2.2. Notice that if the  $\psi_k$ 's are separable, then the error due to finite truncation of the basis systems in Equation (S.1) is  $O(\prod_{d=1}^D w_{\phi_d}(m))$ , and thus the desired result follows. □

**Lemma S5.** Under Assumption 1, if covariance function  $C(\mathbf{x}, \mathbf{y})$  is separable,  $\psi_k$  is a rank-1 MPF for all  $k = 1, 2, \dots, \infty$ .

*Proof.* Denote the eigendecomposition of the marginal covariance functions

$$C_d(x_d, y_d) = \sum_{j=1}^{\infty} \rho_{d,j} \psi_{d,j}(x_d) \psi_{d,j}(y_d).$$

Define  $\psi_k^*(\mathbf{x}) = \prod_{d=1}^D \psi_{d,j_d(k)}(x_d)$ , where  $\mathbf{j}(k) = (j_1(k), \dots, j_D(k))'$  is any one to one mapping between  $k$  and the multi-index. Clearly,  $\langle \psi_k^*, \psi_j^* \rangle_{\mathcal{H}} = \delta_{kj}$ . Additionally, we have

$$\begin{aligned} \int_{\mathcal{M}} C(\mathbf{x}, \mathbf{y}) \psi_k^*(\mathbf{y}) d\mathbf{y} &= \int_{\mathcal{M}} \prod_{d=1}^D C_d(x_d, y_d) \prod_{d=1}^D \psi_{d,j_d(k)}(y_d) dy_1 \cdots dy_D \\ &= \prod_{d=1}^D \int_{\mathcal{M}_d} C_d(x_d, y_d) \psi_{d,j_d(k)}(y_d) dy_d \\ &= \prod_{d=1}^D \int_{\mathcal{M}_d} \sum_{l=1}^{\infty} \rho_{d,j} \psi_{d,l}(x_d) \psi_{d,l}(y_d) \psi_{d,j_d(k)}(y_d) dy_d \\ &= \prod_{d=1}^D \rho_{d,j_d(k)} \psi_{d,j_d(k)} = \left( \prod_{d=1}^D \rho_{d,j_d(k)} \right) \psi_k^*(\mathbf{x}), \end{aligned}$$

which defines  $\psi_k^*$  to be an eigenfunction of  $C$  with corresponding eigenvalue  $\prod_{d=1}^D \rho_{d,j_d(k)}$ . Since  $\mathbf{j}(k)$  is an isomorphism between  $\mathbb{N}$  and itself, this holds for all  $k$ . Furthermore, since  $\mathcal{H}$  is separable, there can only be countably many pairwise orthonormal functions and hence the  $\psi_k^*$ 's are the only eigenfunctions of  $C$ .  $\square$

## S1.4 Proof of Theorem 2.4

*Proof.*

$$\begin{aligned} \sum_{i=1}^N \left\| \mathcal{Y}_i - \sum_{k=1}^K \mathbf{B}_{ik} \bigotimes_{d=1}^D \Phi_d \mathbf{c}_{d,k} \right\|_F^2 &= \left\| \mathcal{Y} - \sum_{k=1}^K \bigotimes_{d=1}^D \Phi_d \mathbf{c}_{d,k} \otimes \mathbf{b}_k \right\|_F^2 \\ &= \left\| \mathcal{Y} - \left[ \sum_{k=1}^K \bigotimes_{d=1}^D \mathbf{D}_d \mathbf{V}'_d \mathbf{c}_{d,k} \otimes \mathbf{b}_k \right] \times_1 \mathbf{U}_1 \times_2 \mathbf{U}_2 \cdots \times_D \mathbf{U}_D \right\|_F^2 \\ &= \left\| \hat{\mathcal{G}} - \left[ \sum_{k=1}^K \bigotimes_{d=1}^D \mathbf{D}_d \mathbf{V}'_d \mathbf{c}_{d,k} \otimes \mathbf{b}_k \right] \right\|_F^2. \end{aligned}$$

Here the first equality is from properties of the Frobenius norm, the second comes from properties of  $d$ -mode multiplication, and the third from invariance of the Frobenius norm to orthogonal transformation. Therefore, solving Equation (14) is equivalent to solving

$$\min_{\mathbf{B}, \mathbf{C}} \left\| \widehat{\mathcal{G}} - \sum_{k=1}^K \bigotimes_{d=1}^D \mathbf{D}_d \mathbf{V}'_d \mathbf{C}_d \otimes \mathbf{b}_k \right\|_F^2. \quad (\text{S.2})$$

Using the mapping  $\widetilde{\mathbf{C}}_d = \mathbf{D}_d \mathbf{V}'_d \mathbf{C}_d$ , Equation (S.2) can be reparameterized as

$$\min_{\mathbf{B}, \widetilde{\mathbf{C}}} \left\| \widehat{\mathcal{G}} - \sum_{k=1}^K \bigotimes_{d=1}^D \widetilde{\mathbf{C}}_d \otimes \mathbf{b}_k \right\|_F^2, \quad (\text{S.3})$$

which is solved by the rank- $K$  CPD of  $\widehat{\mathcal{G}}$ . Comparing Equations (S.2) and (S.3), we see that  $\widehat{\mathbf{B}} = \check{\mathbf{B}}$  and  $\mathbf{D}_d \mathbf{V}_d \widehat{\mathbf{C}}_d = \check{\mathbf{C}}_d$ , or equivalently,  $\widehat{\mathbf{C}}_d = \mathbf{V}_d \mathbf{D}_d^{-1} \check{\mathbf{C}}_d$ .  $\square$

## S2 Algorithm Convergence

Denote  $g(\widetilde{\mathbf{C}}_1, \dots, \widetilde{\mathbf{C}}_D, \mathbf{B})$  as the objective function from problem (16). Algorithm 1 implements a block coordinate descent scheme, where in the  $(r+1)$ 'th iteration the conditional minimization problem

$$\min_{\mathbf{X}} g(\widetilde{\mathbf{C}}_1^{(r+1)}, \dots, \widetilde{\mathbf{C}}_{d-1}^{(r+1)}, \mathbf{X}, \widetilde{\mathbf{C}}_{d+1}^{(r)}, \dots, \widetilde{\mathbf{C}}_D^{(r)}, \mathbf{B}^{(r)})$$

is solved for  $d = 1, \dots, D$ , and likewise for  $\mathbf{B}^{(r+1)}$ . In general, the convergence of such a scheme can be guaranteed if each of the sub-problems is convex and has a unique solution (Bertsekas, 1997). A minor augmentation can be made to the problem which guarantees convergence of the solution sequence,  $\{(\widetilde{\mathbf{C}}_1^{(r)}, \dots, \widetilde{\mathbf{C}}_D^{(r)}, \mathbf{B}^{(r)})\}$ , to a stationary point. In particular, adding a proximal regularization term to obtain the augmented problem

$$\min_{\mathbf{X}} g(\widetilde{\mathbf{C}}_1^{(r+1)}, \dots, \widetilde{\mathbf{C}}_{d-1}^{(r+1)}, \mathbf{X}, \widetilde{\mathbf{C}}_{d+1}^{(r)}, \dots, \widetilde{\mathbf{C}}_D^{(r)}, \mathbf{B}^{(r)}) + \frac{\mu_d^{(r)}}{2} \left\| \mathbf{X} - \widetilde{\mathbf{C}}_d^{(r)} \right\|_F^2 \quad (\text{S.4})$$

where  $\mu_d^{(r)} > 0$ . This can be interpreted as an additional ridge penalty that “shrinks” the solution towards the value at the previous iteration. The augmented problem (S.4) is strongly convex and therefore has a unique solution. If we additionally assume boundedness of the solution sequence, (S.4) is guaranteed to converge to a stationary point of  $g$ . In practice,

boundedness can be enforced by performing normalization to each of the matrices following each iteration of the algorithm. Note that due to the convergence of the solution sequence, the effect of the ridge penalty vanishes as  $r \rightarrow \infty$ .

Solving the augmented problem not only guarantees convergence but has also been shown to improve convergence speed (Li et al., 2013), particularly when  $\mu_d^{(r)}$  is decreased over iterations. Razaviyayn et al. (2013) propose an empirically determined update rule

$$\mu_d^{(r+1)} = \mu_a + \mu_b \frac{\left\| \mathcal{G} - \sum_{k=1}^K \bigotimes_{d=1}^D \tilde{\mathbf{c}}_{d,k}^{(r)} \otimes \mathbf{b}_k^{(r)} \right\|_F}{\|\mathcal{G}\|_F}$$

for some constants small positive constants  $\mu_a, \mu_b$ .

### S3 Two-Stage Multidimensional FPCA Algorithm

Algorithm 2 provides pseudocode for performing the two stage regularized multidimensional FPCA outlined in Section 3. The algorithm requires the precomputation of the marginal inner product matrices defined by

$$\begin{aligned} \mathbf{J}_{\phi_d}(i, j) &= \langle \phi_{d,i}, \phi_{d,j} \rangle_{\mathcal{H}_d} \\ \mathbf{R}_{\phi_d}(i, j) &= \langle \Delta_{\mathcal{M}_d}(\phi_{d,i}), \Delta_{\mathcal{M}_d}(\phi_{d,j}) \rangle_{\mathcal{H}_d} \\ \mathbf{E}_{\phi_d}(i, j) &= \langle \phi_{d,i}, \Delta_{\mathcal{M}_d}(\phi_{d,j}) \rangle_{\mathcal{H}_d} \end{aligned}$$

Given the  $\mathbf{C}_d$ 's, simple derivations show that the marginal product structure of the  $\zeta_k$ 's permits fast analytic computation of  $\mathbf{J}_{\zeta^*}$  and  $\mathbf{R}_{\zeta^*}$  based on the element-wise formulas

$$\mathbf{J}_{\zeta^*}(i, j) = \prod_{d=1}^D \mathbf{c}'_{d,i} \mathbf{J}_{\phi_d} \mathbf{c}_{d,j} \tag{S.5}$$

and

$$\begin{aligned} \mathbf{R}_{\zeta^*}(i, j) &= \sum_{d=1}^D \left( \prod_{b \neq d} \mathbf{c}'_{b,i} \mathbf{J}_{\phi_b} \mathbf{c}_{b,j} \right) \mathbf{c}'_{d,i} \mathbf{R}_{\phi_d} \mathbf{c}_{d,j} \\ &+ \sum_{\substack{a,d \\ a \neq d}} \left( \prod_{\substack{b \neq a \\ b \neq d}} \mathbf{c}'_{b,i} \mathbf{J}_{\phi_b} \mathbf{c}_{b,j} \right) (\mathbf{c}'_{d,i} \mathbf{E}_{\phi_d} \mathbf{c}_{d,j}) (\mathbf{c}'_{a,i} \mathbf{E}_{\phi_a} \mathbf{c}_{a,j}). \end{aligned} \tag{S.6}$$

In practice, we form estimates  $\widehat{\mathbf{C}}_d$  using Algorithm 1. The corresponding estimates of the inner product matrices  $\widehat{\mathbf{J}}_{\zeta^*}$  and  $\widehat{\mathbf{R}}_{\zeta^*}$  are obtained by plugging  $\widehat{\mathbf{C}}_d$  into (S.5) and (S.6), respectively.

We offer a couple quick remarks on the practical implementation of Algorithm 2. There are several ways to solve the generalized eigenvalue problem (29). We used Algorithm 9.4.2 in Ramsay (2005), since it avoids direct construction of  $\Sigma_{\mathbf{b}}$  which is important for numerical stability in the high dimensional case when  $K > N$ . If subsequent dimensionality reduction is desirable, an initial  $K$ -MPB with a very large  $K$  can be estimated and then used to construct the basis system  $\{\psi_1, \dots, \psi_{K^*}\}$ , where  $K^* < K$  can be chosen by a threshold on the desired proportion of variance explained. In practice, it is often the case that a  $K^* \ll K$  can explain a large proportion of the functional variance, see Section 5 for an example.

---

**Algorithm 2** Two-Stage Regularized Multidimensional FPCA

---

- 1: Estimate  $\{\tilde{\mathbf{C}}_d\}$ ,  $\hat{\mathbf{B}}$  using Algorithm 1
  - 2: Transform  $\hat{\mathbf{C}}_d = \mathbf{V}'_d \mathbf{D}_d^{-1} \tilde{\mathbf{C}}_d$  for  $d = 1, \dots, D$
  - 3: Assemble  $\hat{\mathbf{J}}_{\zeta^*}$  and  $\hat{\mathbf{R}}_{\zeta^*}$  using (S.5) and (S.6), respectively.
  - 4: Compute  $\hat{\mathbf{S}} = [\mathbf{s}_1, \dots, \mathbf{s}_{K^*}]$  using Algorithm 9.4.2 in Ramsay (2005).
- 

## S4 Data Adaptive Marginal Basis

In the following, we develop an alternative framework to estimating  $\xi_{k,d}$  over a prespecified  $\phi_d$  in which the marginal basis systems are allowed to be data adaptive.

### S4.1 Overview of Random Projections

Our construction of a data adaptive marginal basis system is built off of the framework of random projections. The utility of random projection techniques for performing decomposition of large matrices is elaborated in the influential work of Halko et al. (2011). Given a matrix  $\mathbf{A} \in \mathbb{R}^{m \times n}$ , where  $m$  and  $n$  are large, random projection methods aim to construct an optimal rank  $r \ll \min(m, n)$  subspace, spanned by the columnwise orthogonal  $\mathbf{U} \in \mathbb{R}^{m \times r}$ , such that

$$\mathbf{A} \approx \mathbf{U}\mathbf{U}'\mathbf{A}.$$

Whatever downstream matrix decomposition is of interest can instead be approximated by applying it to the projected matrix  $\mathbf{U}'\mathbf{A}$ , at a much lower computational cost.

So how is  $\mathbf{U}$  formed? This is where randomness becomes useful. Define the random vector  $\mathbf{z} \in \mathbb{R}^n$  whose elements are, for example, *i.i.d.* standard normal. Forming a sample of  $r$  realizations of  $\mathbf{z}$ , randomness ensures with high probability that the set of sample vectors  $\{\mathbf{z}_i : i = 1, \dots, r\}$  are both in general linear position and linearly independent. As a result, the set of transformed random vectors  $\{\mathbf{A}\mathbf{z}_i : i = 1, \dots, r\}$  are both non-zero and linearly independent. If the rank of  $\mathbf{A}$  is exactly  $r$ , then the set of transformed vectors will span its columnspace with high probability and therefore  $\mathbf{U}$  can be constructed by forming an orthogonal basis for the set, e.g. by the QR-decomposition. Rather than having exactly rank  $r$ , it is often more reasonable to assume that  $\mathbf{A}$  can be decomposed into the sum of a rank  $r$  matrix (the signal) and a residual matrix with relatively small expected norm (the noise). In this case, it can actually be beneficial to draw more than  $r$  samples of  $\mathbf{z}$  in order to fully interrogate the columnspace of the low rank signal, due to the effect of the residual component (Halko et al., 2011).

## S4.2 Reformulating the Loss

Consider the objective function of the optimization problem (16). Notice that the loss term depends on  $\phi_d$  only through  $\mathbf{U}_d$ , i.e. in the construction of  $\widehat{\mathcal{G}}$ . Therefore, we can recast the problem of selecting a set of optimal marginal basis systems as the problem of selecting a set of  $\mathbf{U}_d$  that, in some sense, produce an optimal compression of  $\mathcal{Y}$ . We propose to form  $\mathbf{U}_d$  using random projections applied to the corresponding  $d$ -mode matricization  $\mathcal{Y}$ .

The proposed procedure is outlined in Algorithm 3, which is essentially a combination of Algorithms 4.2 and 4.4 from Halko et al. (2011). The first for loop implements power iterations in order to increase the decay rate of the spectrum of the  $\mathbf{Y}_{(d)}$  while retaining the same singular vectors. Data adaptive selection of the marginal ranks  $m_d$  is then performed in the while loop and is guided by the tuning parameter  $\text{tol}$ , which ensures  $m_d$  is large enough that

$$\|(\mathbf{I} - \mathbf{U}_d \mathbf{U}_d') \mathbf{Y}_{(d)}\|_F < \text{tol}.$$

with probability at least  $1 - 10^{-r}$  (Halko et al., 2011).

We note that a variety of randomized methods have been developed to perform tensor

---

**Algorithm 3** Data-driven  $\mathbf{U}_d$  via Random Projections

---

```
1: Input  $\mathbf{Y}_{(d)}$ , tol, q, r
2: Output  $\mathbf{U}_d$ 
3: Initialize  $\mathbf{U}_d$  as an empty  $n_d \times 0$  matrix,  $j = 1$ 
4: Sample  $n_d$   $\mathbf{z}_i \sim \mathcal{N}(\mathbf{0}, \mathbf{I})$  of length  $N \prod_{j \neq d} n_j$ 
5:  $\mathbf{A}_d = \mathbf{Y}_{(d)}[\mathbf{z}_1, \dots, \mathbf{z}_d]$ 
6: for  $l=1, \dots, q$  do
7:   From the LU-decomposition  $\mathbf{L}_{lower}, \mathbf{U}_{upper} = \text{lu}(\mathbf{A}_d)$ 
8:   Form the LU-decomposition of the product  $\mathbf{L}_{lower}, \mathbf{U}_{upper} = \text{lu}(\mathbf{Y}'_{(d)} \mathbf{L}_{lower})$ 
9:    $\mathbf{A}_d = \mathbf{Y}_{(d)} \mathbf{L}_{lower}$ 
10: while  $\max\{\|\mathbf{A}_d(:, j)\|, \dots, \|\mathbf{A}_d(:, j+r-1)\|\} \geq \text{tol} \|\mathbf{A}_d\|_F / (10\sqrt{2\pi})$  do
11:    $\mathbf{A}_d(:, j) = [\mathbf{I} - \mathbf{U}_d(:, 1:j-1) \mathbf{U}'_d(:, 1:j-1)] \mathbf{A}_d(:, j)$ 
12:    $\mathbf{U}_d(:, j) = \mathbf{A}_d(:, j) / \|\mathbf{A}_d(:, j)\|$ 
13:    $\mathbf{A}_d(:, j+r) = [\mathbf{I} - \mathbf{U}_d(:, 1:j) \mathbf{U}'_d(:, 1:j)] \mathbf{A}_d(:, j+r)$ 
14:   for  $l=j+1, \dots, j+r-1$  do
15:      $\mathbf{A}_d(:, l) = \mathbf{A}_d(:, l) - \langle \mathbf{A}_d(:, l), \mathbf{U}_d(:, j) \rangle \mathbf{U}_d(:, j)$ 
16:    $j = j + 1$ 
```

---

decomposition, including subsampling (Battaglino et al., 2018) and randomized projection techniques (Erichson et al., 2020). Algorithm 3 is similar to Algorithm 1 from Erichson et al. (2020), except the latter prespecifies a single parameter for all of the marginal ranks and uses oversampling to accommodate for noise, as opposed to the proposed scheme which permits the data adaptive selection of marginal ranks controlled by a relative error tolerance parameter.

### S4.3 Regularization

Although the loss term in (16) can be formulated in a manner agnostic to  $\phi_d$ , the roughness penalty depends on the smoothness of the candidate estimates, quantified by  $\mathbf{T}_d$  which, under the construction given in the proof to Proposition 2.6, depends explicitly on  $\phi_d$ . We now describe a technique to estimate  $\mathbf{T}_d$  without explicitly specifying  $\phi_d$ .

Let  $Q_d$  be a quadrature rule with

$$\int_{\mathcal{M}_d} h(x_d) = \sum_{l=1}^{q_d} w_{d,l} h(x_{d,l}) + E(h),$$

where  $\{(w_{d,l}, x_{d,l})\}$  are the weights and points defining the quadrature rule,  $h$  is the function to be integrated and  $E(h)$  is the error term of the approximation, which depends on both  $Q_d$  and  $h$ . Let  $\mathbf{L}_{d,Q} \in \mathbb{R}^{q_d \times n_d}$  be the estimates of differential operator  $L_d(h)$  at the quadrature points in  $Q_d$  based on the point evaluations of  $h$  over  $\mathbf{x}_d$ . In the simplest case, the points in  $Q_d$  are the same as the equispaced marginal grid points and then  $\mathbf{L}_{d,Q}$  may be formed using finite differences with the appropriate stencil over  $\mathbf{x}_d$ . In general, it may be desirable to specify a quadrature rule over a different grid, for example if  $\mathbf{x}_d$  is very dense, in which case (linear) imputation would be necessary to form the desired estimates at the quadrature points. In any case, we can form an estimate for the marginal roughness penalty by plugging in the following estimator of  $\mathbf{T}_d$

$$\widehat{\mathbf{T}}_d = \mathbf{U}'_d \mathbf{L}'_{d,Q} \mathbf{Q}_d \mathbf{L}_{d,Q} \mathbf{U}_d, \tag{S.7}$$

where  $\mathbf{Q}_d = \text{Diag}(w_{d,1}, \dots, w_{d,q_d})$  is the diagonal matrix of numerical quadrature points.

## S4.4 Obtaining a Continuous Representation

In the proposed adaptive marginal basis methodology, instead of specifying  $\boldsymbol{\phi}_d$  directly, we form a data driven estimate of  $\mathbf{U}_d$  using Algorithm 3 along with the discretized estimate of  $\mathbf{T}_d$  using the method outlined in Section S4.3. These quantities can then be used in Algorithm 1 to construct  $\tilde{\mathbf{C}}_d$ . In the context of our model, recall that

$$\boldsymbol{\Xi}_d = \boldsymbol{\Phi}_d \mathbf{C}_d = \mathbf{U}_d \tilde{\mathbf{C}}_d,$$

therefore we can form estimates of the optimal marginal basis function evaluations at each of the marginal grid points. To obtain the final continuous representations of  $\xi_{d,k}$ , a marginal function approximation, e.g. smoothing or interpolation, is performed.

## S5 Additional Simulation Studies

### S5.1 Overview of Sandwich Smoother

The so-called *sandwich smoother*, first introduced by Xiao et al. (2013) and then extended by French and Kokoszka (2021), is a method for estimating the coefficients of a tensor product approximation to an unknown deterministic function from noisy observations on a grid. The main contribution is in a clever formulation of the penalty term, which allows for the fast computation of the GCV statistic and hence a computationally efficient technique for selecting the roughness penalty strength. For more information, see either of the aforementioned papers or the `hero` package in R (French, 2020).

### S5.2 Overview of FCP-TPA

We give a brief overview of the the FCP-TPA algorithm (Allen, 2013), which is essentially a  $D$ -dimensional extension of the 2-dimensional regularization scheme from Huang et al. (2009). As such, it does not consider the same problem that the current work explores, namely optimal basis systems for representing a random sample of functional data. Rather they consider the canonical nonparametric function approximation task, in which there is a single, unknown deterministic function discretely observed with error. That said, it is easy enough to adapt their method to our situation, i.e. by introducing a non-smooth “subject mode”. This is what is presented below.

Using our notation, the FCP-TPA estimates the  $k$ th *MPF basis evaluation vectors*  $\Xi_{d,k}$  and associated coefficient vector  $\mathbf{b}_k$  by solving a series of  $K$  rank-one penalized decompositions of the residual tensor. That is, at the  $k$ th iteration, FCP-TPA solves problem

$$\min_{\Xi_{1,k}, \dots, \Xi_{D,K}, \mathbf{b}_k} \left\| \mathcal{Y}_{resid} - \bigotimes_{d=1}^D \Xi_{d,k} \otimes \mathbf{b}_k \right\|_F^2 - \prod_{d=1}^D \left\| \Xi_{d,k} \right\|_2^2 + \prod_{d=1}^D \Xi'_{d,k} \mathbf{P}_d^{-1} \Xi_{d,k} \quad (\text{S.8})$$

where  $\mathcal{Y}_{resid} = \mathcal{Y} - \sum_{j=1}^{k-1} \bigotimes_{d=1}^D \Xi_{d,j} \otimes \mathbf{b}_j$  and  $\mathbf{P}_d \in \mathbb{R}^{n_d \times n_d}$  is a smoothing matrix, e.g. derived using squared second order differences. The solution to (S.8) is approximated using tensor power iterations, which are shown to converge to a stationary point.

Note that FCP-TPA does not directly construct a continuous representation but rather the discrete evaluations of the optimal marginal product functions on the observed marginal

grid, i.e. the  $\Xi_d$ 's. In order to obtain a continuous representation from the output of FCP-TPA, the decompose-then-represent approach is used in which the marginal basis functions are estimated from the basis expansion of the  $\Xi_d$ 's.

### S5.3 Representing a Random Sample

Table S1 displays a comparison of the performance of the  $K$ -oMPB estimated by Algorithm 1 (denoted **MARGARITA**) and the tensor product basis estimated by the sandwich smoother. For all combinations of distribution and sampling plans considered, **MARGARITA** exhibits lower moMISE over the sample than the tensor product basis when comparing models with similar number degrees of freedom. **MARGARITA** is often able to produce better fits than the tensor product basis with substantially fewer degrees of freedom. For example, the  $K$ -oMPB with 675 degrees of freedom exhibits lower moMISE than the tensor product basis system with 2,197 degrees of freedom for all considered settings.

The strong performance of the **MARGARITA** is driven at least in part by the ability to share information across the sample to estimate a set of basis functions that conforms to the distribution. From table S1, we can see this is of particular importance in the case of low SNR, for which access to a larger sample size,  $N = 50$  vs.  $N = 5$ , typically results in significantly lower moMISE. A caveat here is that for the gain from information pooling to be realized, the rank of the model must be “large enough”, e.g. compare results from  $K_{fit} = 8$  to the  $K_{fit} = 15, 25$  case. This is a distinct advantage over the tensor product basis system, whose estimation is done for each subject independently.

Table S2 displays the relative difference in moMISE, defined as

$$\frac{\text{moMISE}_{\text{FCP-TPA}} - \text{moMISE}_{\text{MARGARITA}}}{\text{moMISE}_{\text{FCP-TPA}}} \quad (\text{S.9})$$

between the fits resulting from the FCP-TPA algorithm and **MARGARITA**. As all but one of the entries in the table is positive, **MARGARITA** is nearly uniformly outperforming the FCP-TPA. The one configuration for which FCP-TPA has lower moMISE is the low SNR, small sample size along with large marginal rank  $m_d = 25$ , which is somewhat pathological and both methods perform poorly. Echoing results in Section 4.1, we see the boost in performance from **MARGARITA** generally increases with  $K_{fit}$ .

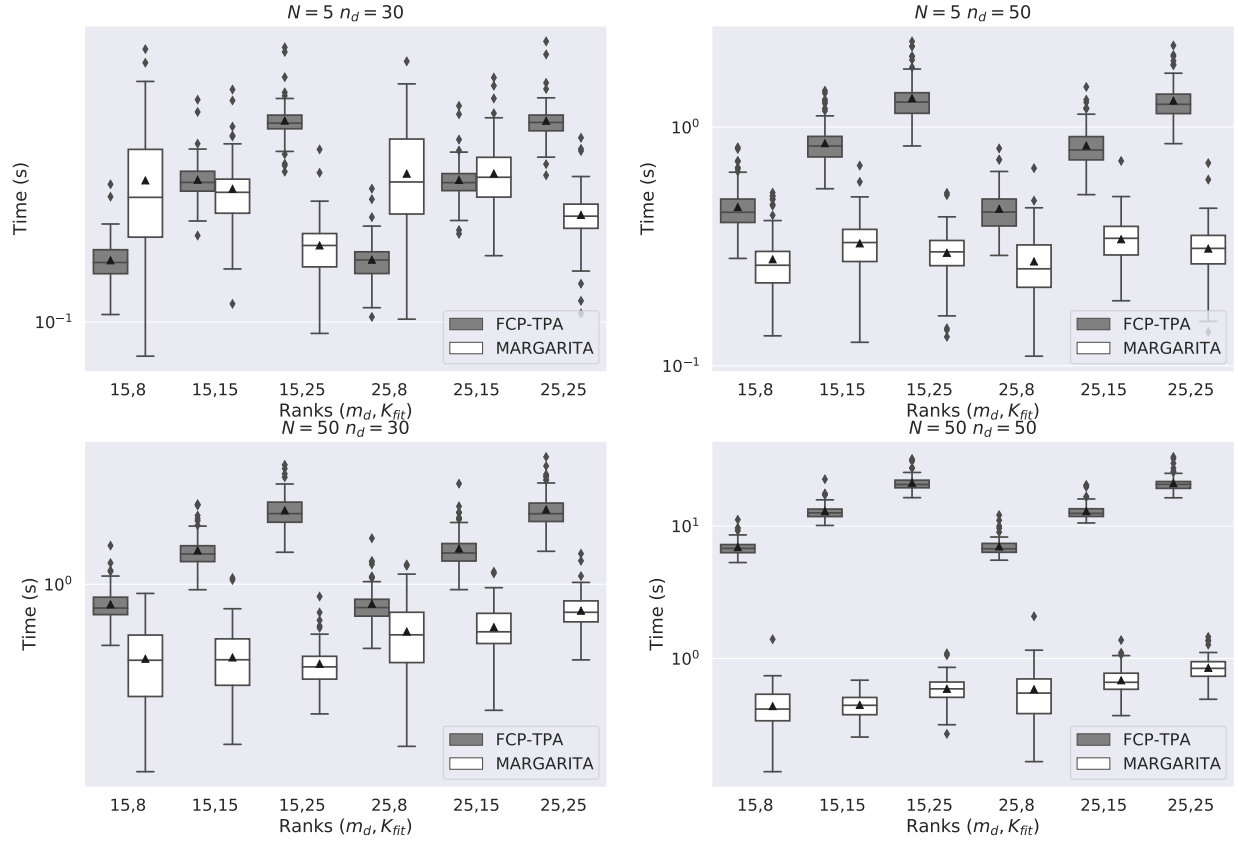


**Figure S1:** Computational time comparison between FCP-TPA and MARGARITA. The Y-axis is plotted on log-scale for clarity.

Figure S1 shows a computational time comparison between the two algorithms. For all panels, we fixed  $K_t = 20$  and  $\sigma^2 = 10.0$ , but similar patterns emerge for the other cases. For most cases MARGARITA is faster than FCP-TPA, the only exceptions being for very small sample size and small ranks, which may be considered as toy examples.

**Table S1:** moMISE comparison of MARGARITA (a), to the tensor product basis estimated by sandwich smoother from Xiao et al. (2013) (b), for a variety of distributions and samplings configurations. The penalty parameter for the former is selected through a grid search and for the latter by minimizing a GCV criterion.

(a) Marginal Product Basis

$K_{true}$	$\sigma^2$	$N$	$n_d$	$K_{fit} = 15$			$K_{fit} = 25$		
				$m_d$ (model d.o.f.)					
				8 (360)	15 (675)	25 (1,125)	8 (600)	15 (1,125)	25 (1,875)
10	0.5	5	30	0.0890	0.0433	0.0433	0.0511	0.0030	0.0033
10	0.5	5	50	0.0932	0.0405	0.0402	0.0560	0.0006	0.0006
10	0.5	50	30	0.1186	0.0426	0.0411	0.0790	0.0017	0.0007
10	0.5	50	50	0.1196	0.0398	0.0394	0.0757	0.0001	0.0001
10	10.0	5	30	0.1148	0.1049	0.1634	0.1039	0.0919	0.1579
10	10.0	5	50	0.0976	0.0530	0.0647	0.0616	0.0180	0.0312
10	10.0	50	30	0.1166	0.0525	0.0632	0.0800	0.0146	0.0263
10	10.0	50	50	0.1149	0.0423	0.0441	0.0745	0.0019	0.0033
20	0.5	5	30	0.4910	0.1158	0.0684	0.4418	0.0511	0.0059
20	0.5	5	50	0.4872	0.1075	0.0627	0.4429	0.0475	0.0015
20	0.5	50	30	0.6334	0.1239	0.0679	0.5850	0.0564	0.0025
20	0.5	50	50	0.6388	0.1182	0.0646	0.5998	0.0539	0.0009
20	10.0	5	30	0.5058	0.1587	0.1723	0.4736	0.1200	0.1492
20	10.0	5	50	0.4994	0.1185	0.0841	0.4534	0.0594	0.0286
20	10.0	50	30	0.6544	0.1353	0.0867	0.6008	0.0682	0.0220
20	10.0	50	50	0.6415	0.1231	0.0674	0.5915	0.0579	0.0039

(b) Tensor Product Basis

$K_{true}$	$\sigma^2$	$N$	$n_d$	$m_d$ (model d.o.f.)					
				7 (343)	8 (512)	9 (729)	11 (1,331)	12 (1,728)	13 (2,197)
10	0.5	5	30	1.1409	0.9520	0.9096	0.5327	0.4817	0.2136
10	0.5	5	50	1.1251	0.9326	0.8870	0.5067	0.4581	0.1823
10	0.5	50	30	1.1457	0.9556	0.9130	0.5338	0.4840	0.2134
10	0.5	50	50	1.1170	0.9251	0.8789	0.5020	0.4516	0.1832
10	10.0	5	30	1.1579	1.0224	1.0136	0.7705	0.7559	0.6051
10	10.0	5	50	1.1476	0.9677	0.9300	0.5822	0.5492	0.3027
10	10.0	50	30	1.1822	1.0465	1.0369	0.7861	0.7721	0.6109
10	10.0	50	50	1.1518	0.9679	0.9334	0.5857	0.5517	0.3036
20	0.5	5	30	1.8024	1.6254	1.4738	0.9819	0.7065	0.3806
20	0.5	5	50	1.7445	1.5693	1.4194	0.9342	0.6623	0.3464
20	0.5	50	30	1.8352	1.6530	1.4973	1.0030	0.7218	0.3842
20	0.5	50	50	1.8207	1.6349	1.4739	0.9748	0.6911	0.3580
20	10.0	5	30	1.8076	1.6757	1.5688	1.2221	1.0375	0.8092
20	10.0	5	50	1.8592	1.6807	1.5290	1.0597	0.7971	0.4817
20	10.0	50	30	1.9789	1.8289	1.7073	1.3210	1.1113	0.8472
20	10.0	50	50	1.8527	1.6765	1.5280	1.0560	0.7946	0.4833

**Table S2:** Relative difference in moMISE, as defined by equation (S.9), for FCP-TPA (Allen, 2013) and MARGARITA for marginal ranks 15 and 25 and  $K_{fit} = 8, 15, 25$ . Positive values indicate lower moMISE for MARGARITA. A grid search to select  $\lambda_d$  was performed for each fit and the results from the optimal value are reported. The entry in bold face indicates the **only case** that FCP-TPA outperformed MARGARITA.

$K_{true}$	$\sigma^2$	$N$	$n_d$	$K_{fit} = 15$			$K_{fit} = 25$		
				$m_d$					
				8	15	25	8	15	25
10	0.5	5	30	0.2113	0.2506	0.1738	0.3062	0.7949	0.7160
10	0.5	5	50	0.2544	0.2433	0.1534	0.3634	0.9328	0.8518
10	0.5	50	30	0.2062	0.2118	0.1555	0.2323	0.9228	0.8734
10	0.5	50	50	0.1597	0.1850	0.1167	0.2954	0.9757	0.9437
10	10.0	5	30	0.3684	0.2533	<b>-0.0770</b>	0.4413	0.4426	0.4895
10	10.0	5	50	0.3086	0.3824	0.2120	0.4409	0.6580	0.4486
10	10.0	50	30	0.3487	0.3509	0.1540	0.3529	0.6836	0.5607
10	10.0	50	50	0.2080	0.3300	0.2446	0.3079	0.7229	0.7629
20	0.5	5	30	0.0946	0.4304	0.4429	0.1152	0.6157	0.8706
20	0.5	5	50	0.1139	0.4149	0.4505	0.1243	0.6088	0.9428
20	0.5	50	30	0.0708	0.4452	0.4624	0.0743	0.6107	0.9699
20	0.5	50	50	0.0835	0.4274	0.4554	0.0880	0.6092	0.9816
20	10.0	5	30	0.1235	0.4651	0.3642	0.1385	0.5306	0.6020
20	10.0	5	50	0.1329	0.4600	0.5117	0.1382	0.5928	0.7476
20	10.0	50	30	0.0954	0.4489	0.5313	0.0753	0.5856	0.8161
20	10.0	50	50	0.0915	0.4349	0.5089	0.0983	0.6155	0.9299

## S5.4 Evaluating Multidimensional FPCA

In this section we evaluate the proposed two-stage methodology for estimating the eigenfunctions of multidimensional random function  $U$ . We define a non-stationary anisotropic covariance function  $C(x, y)$  over  $\mathcal{M} = [0, 1]^2$  by specifying its eigenvalues and eigenfunctions. For the latter, a tensor product basis system,  $\phi_1 \otimes \phi_2$ , is constructed using cubic B-splines defined over equispaced knots on each marginal space. An eigen-decomposition of the pairwise  $\mathbb{L}^2$  inner product matrix, denoted  $\mathbf{J}_{\phi_1 \otimes \phi_2} = \mathbf{P}\mathbf{\Gamma}\mathbf{P}'$ , is computed and used to define the coefficients of the eigenfunctions according to  $\boldsymbol{\psi} = \mathbf{\Gamma}^{-1/2}\mathbf{P}'\text{vec}(\phi_1 \otimes \phi_2)$ . The  $k$ th eigenvalue is defined as  $\rho_k = \exp(-0.5k)$ .  $N$  realizations of  $U$  are simulated using a Gaussian process assumption, i.e. a  $\mathcal{N}(0, \rho_k)$  distribution on the coefficients of the  $\psi_k$ 's. Each realizations is evaluated on an equispaced  $100 \times 100$  grid on  $\mathcal{M}$  and subsequently collected to form the observed data tensor  $\mathcal{Y}$ .

MARGARITA is used to estimate  $K$ -oMPB for several ranks  $K$ . For simplicity,  $\phi_1$  and  $\phi_2$  are used as the marginal basis for fitting. The second order derivative operator is used to define the marginal roughness penalty and the coefficients are penalized with a ridge penalty. Since we do not add *i.i.d.* noise to the observations, small penalty strengths are used. The estimated  $K$ -oMPB are then used to estimate the eigenfunctions according to methods in Section 3.

Figure S2 displays heat-maps of the top 3  $K$ -oMPB (left column) and the top 3 estimated eigenfunctions (right column) for  $K = 30$  and  $N = 100$ . Notice that the separable structure of the marginal product basis functions results in highly regular, checkered-like designs. This highlights an important feature of  $K$ -oMPB: the ability to learn the optimal simple spatial patterns from data that can linearly combine to approximate much more complicated functions. The eigenfunctions, being linear combinations of the  $K$ -oMPB, are not separable and therefore exhibit less rigid, more irregular spatial patterns. Figure S3 shows the surface plots of the top 3 estimated eigenfunctions (left column) compared to the true eigenfunctions (right column). Visual inspection affirms that our 2-stage method produces strong fits.

Of course, the quality of the results are dependent both on having an adequate training sample  $N$  and choosing a sufficiently large  $K$ . This fact is illustrated in Figures S4 and

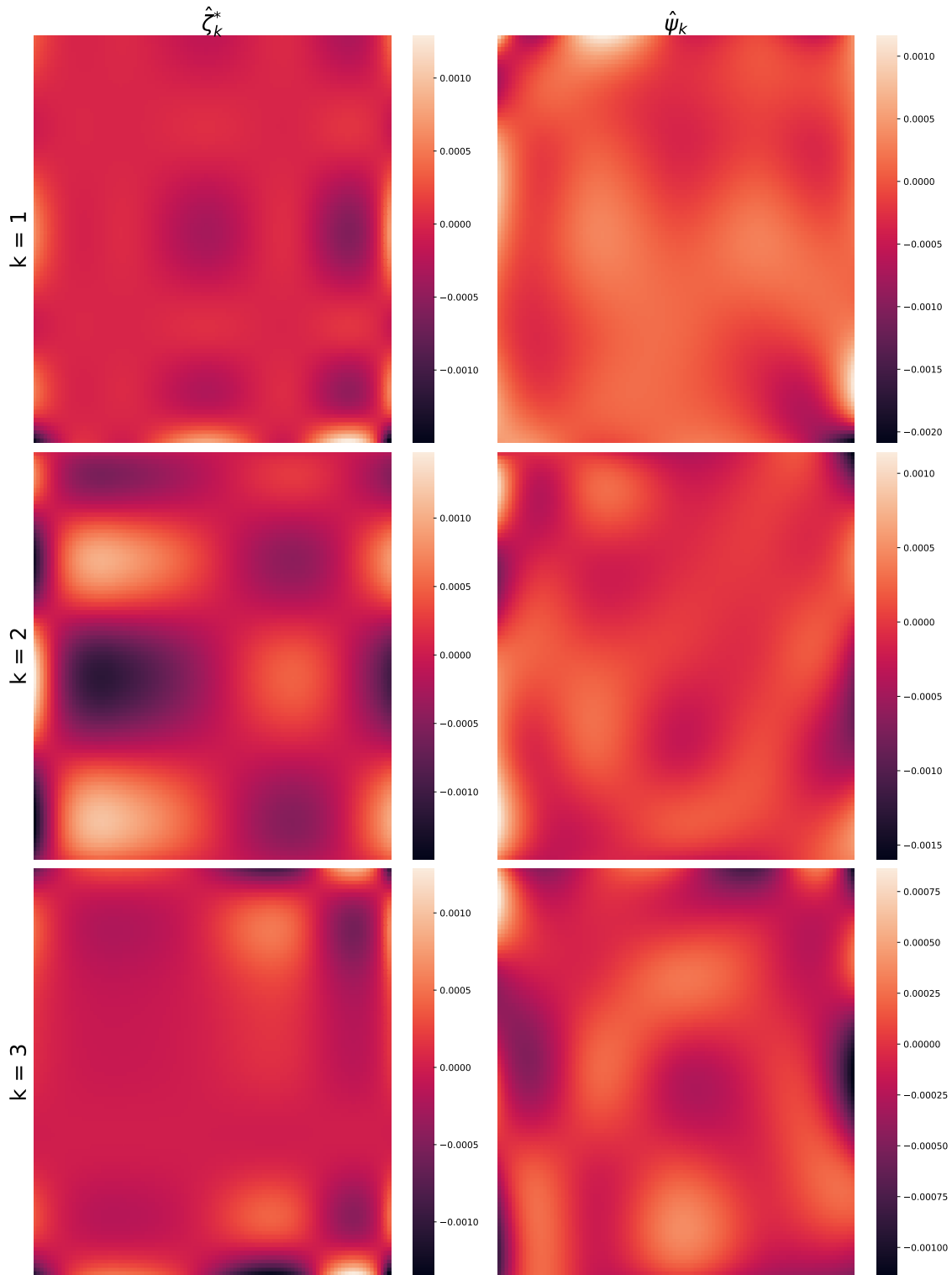


**Figure S2:** First 3  $K$ -MPF basis (left column) and estimated eigenfunctions (right column) for  $N = 100, K = 30$ .

S5, which display the same information as Figure S3 for the case of  $N = 100, K = 10$  and  $N = 20, K = 10$ , respectively. The estimates of the eigenfunctions degrade when the  $K$  isn't taken sufficiently large and then further when the sample size  $N$  is too small. Eventually, we plan to derive a principled, data-driven criterion to select  $K$ . In practice, due to the computational efficiency of **MARGARITA**, we suggest that the user is liberal with their specification of  $K$ , opting for large values to capture as much signal as possible. If further dimensionality reduction is required, Algorithm 2 incurs trivial computational cost even for moderately large  $K$  and thus can be computed essentially for free.

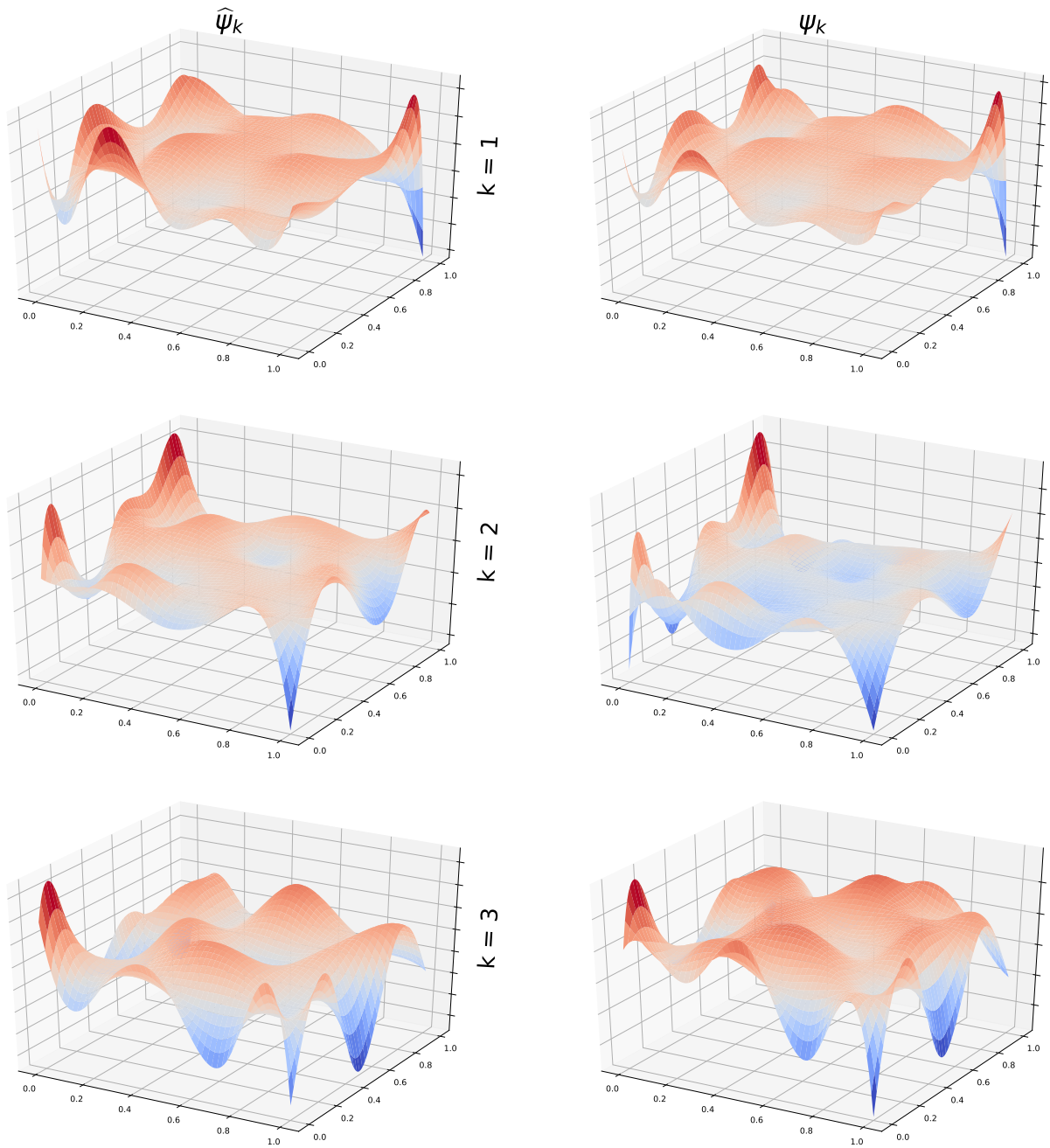


**Figure S3:** First 3 estimated (left column) vs. true (right column) eigenfunctions for  $N = 100, K = 30$ .

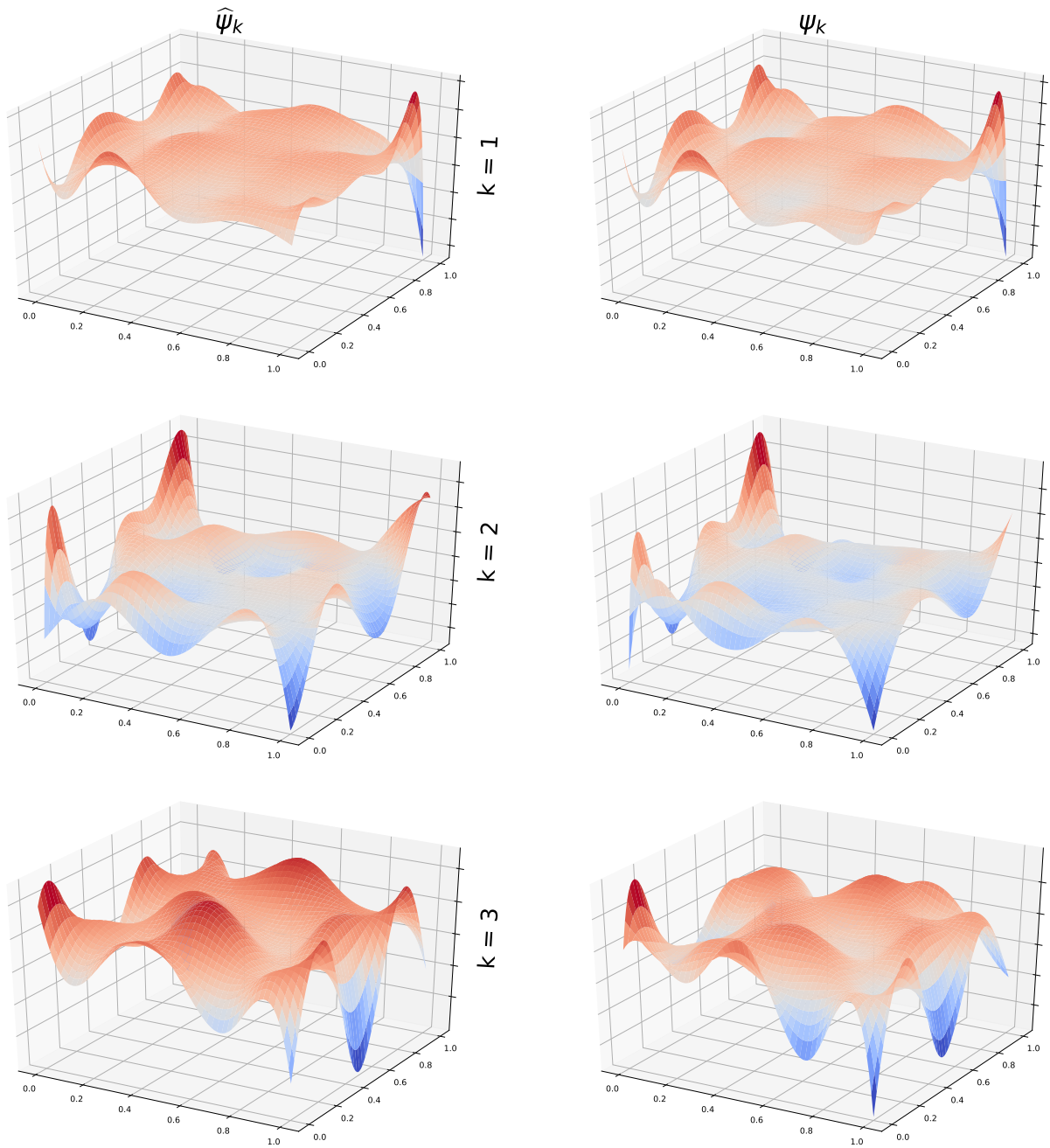


**Figure S4:** First 3 estimated (left column) vs. true (right column) eigenfunctions for  $N = 100, K = 10$ .

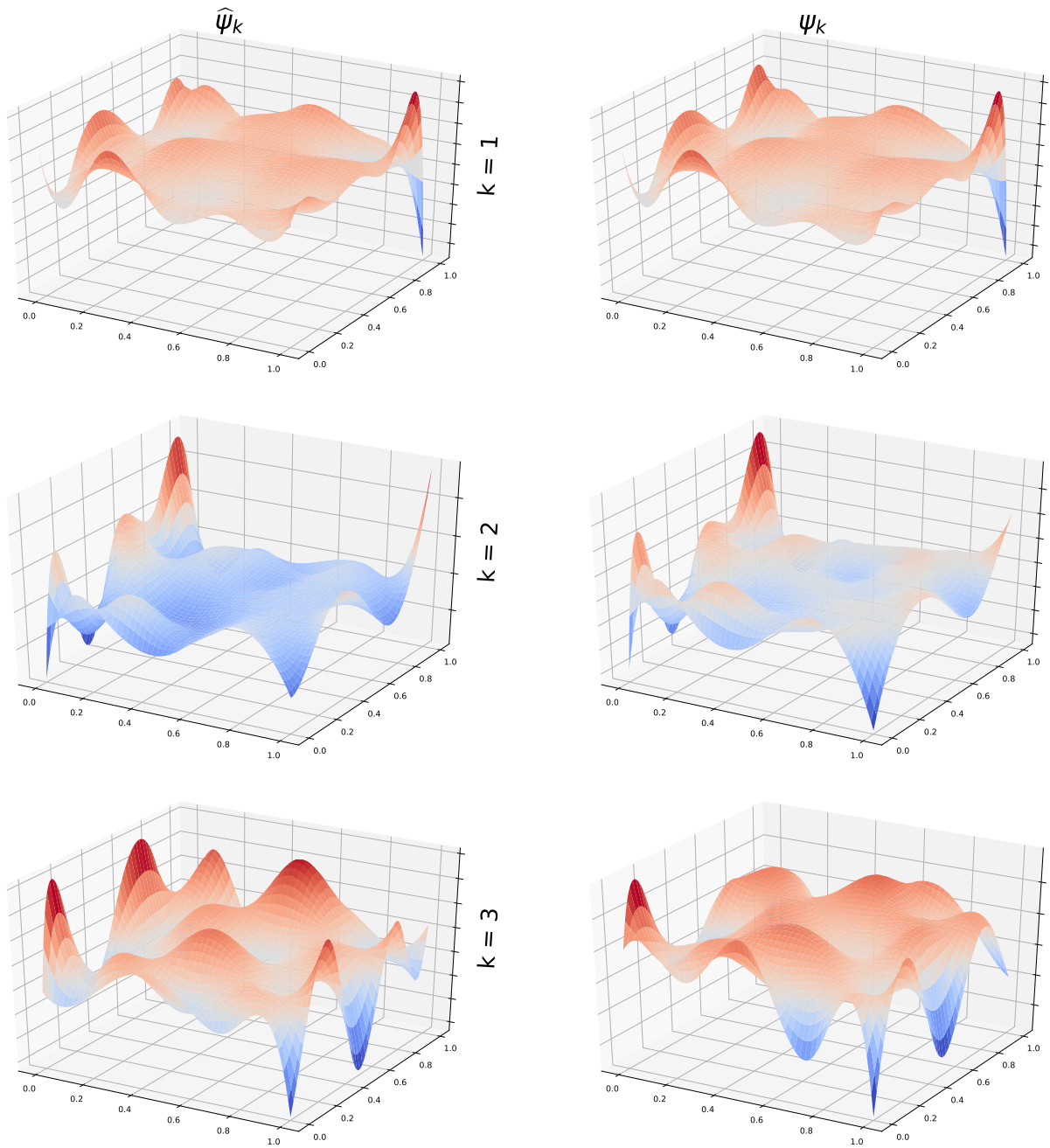


**Figure S5:** First 3 estimated (left column) vs. true (right column) eigenfunctions for  $N = 20, K = 30$ .

## S5.5 Analytic Functions

In this section, we briefly demonstrate the proposed methods utility for a different but related task, that of approximating the output of a (deterministic) analytic test function. The proposed framework is easily adapted to this situation by setting the subject mode dimension to 1. We evaluate our method on the benchmark Friedman 2 and 3 functions, which have the analytic form

$$y_i = \sqrt{x_{1i}^2 + \left(x_{2i}x_{3i} - \frac{1}{x_{2i}x_{4i}}\right)^2}$$

and

$$y_i = \arctan\left(\frac{x_{2i}x_{3i} - (x_{2i}x_{4i})^{-1}}{x_{1i}}\right)$$

respectively, where  $\mathcal{M} = [0, 100] \times [40\pi, 560\pi] \times [0, 1] \times [0, 11]$ . A total of  $n_1 = n_2 = n_3 = n_4 = 20$  equispaced observations are sampled in each marginal dimension. A marginal basis system of cubic B-splines is selected for modeling.

For the Friedman 2 function, with only 5 marginal basis functions in each dimension, a rank-1 marginal product basis model is able to obtain an  $r^2 \approx 0.998$ . Using the same set-up for Friedman 3 function approximation, the resulting model fit has an  $r^2 \approx 0.813$ . We are able to increase this  $r^2 > 0.99$  by doubling the number of marginal cubic B-splines to 10 and increasing the rank to 5.

We also consider the performance of the marginal product basis estimated by **MARGARITA** on a standard nonparametric regression task, with deterministic but unknown regression function and additive Gaussian errors. In the context of the current work, this task may correspond to estimating the mean function of  $U$  from the pooled data tensor. Specifically, we use the observation model

$$y_i = \gamma\left(x_{2i} - x_{1i}\left(\frac{1}{3}x_{1i}^2 - 3\right)\right) + \epsilon_i,$$

where  $\gamma$  is the standard normal density function. The performance of **MARGARITA** is compared with tensor product basis estimation, from here on abbreviated TPB, and generalized additive model, denoted GAM. In order to facilitate fair comparison between the models, we enforce the total number of parameters to be roughly equivalent. To this end, for **MARGARITA**  $K$  is

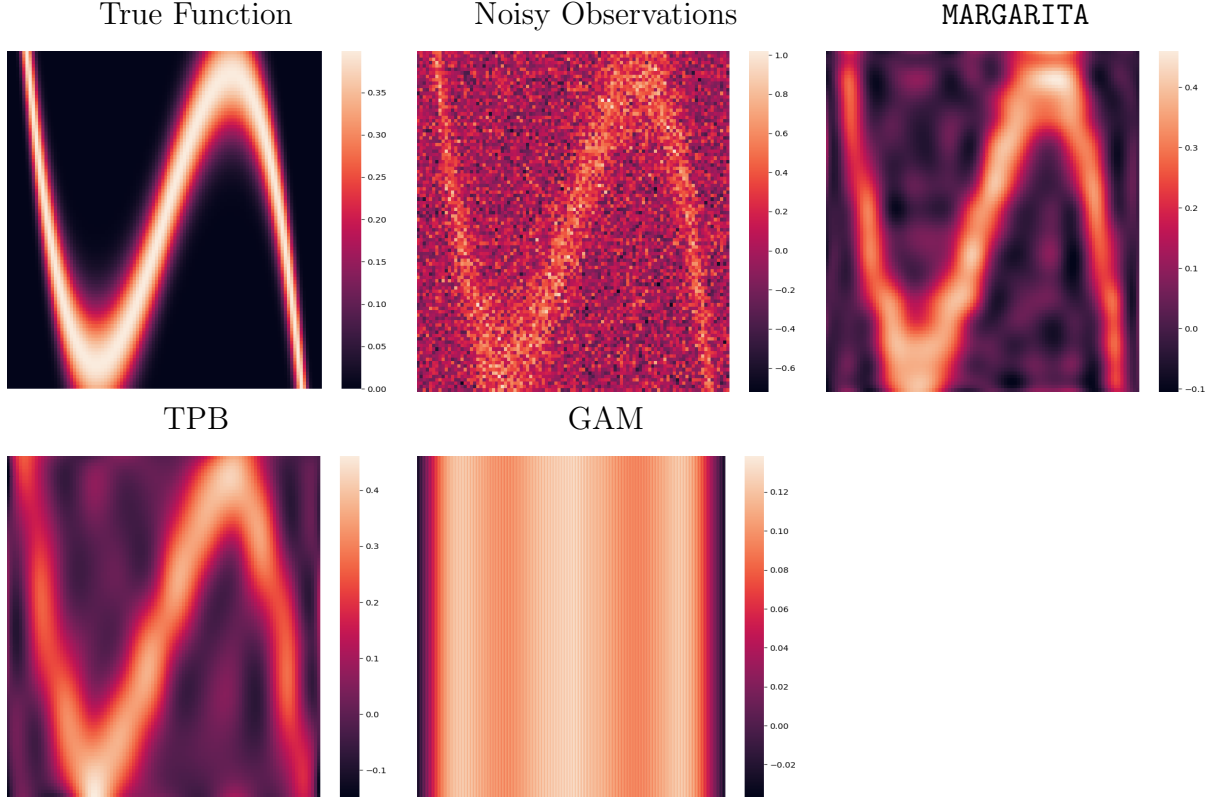


**Figure S6:** Comparison of MARGARITA, TPB and GAM fits for the canonical non-parametric regression task, for a highly non-linear unknown function.

set to 5 and cubic B-splines of rank 18 are used for the marginal basis systems, giving a total of 180 parameters to estimate. Cubic B-splines are also used for the TPB and GAM models, with 14 in each marginal direction for the TPB (196 total parameters) and 90 in each dimension for the GAM (180 total parameters). TPB is estimated via the sandwich smoothing technique from Xiao et al. (2013), implemented in the hero package (French, 2020). The GAM is estimated using the `mgcv` package (Wood, 2011). The smoothing parameters for both the TPB and GAM models were chosen using a GCV criteria, while a grid search is performed to select the marginal smoothing parameters in MARGARITA. The domain is set to be  $\mathcal{M} = [-4, 4]^2$  and samples were taken on a regular grid constructed from 100 equispaced points in each marginal direction.

Figure S6 shows heatmaps of the true function, noisy observations and fits from each of the models considered. The MARGARITA fit resulted in the lowest root mean squared error (RMSE) from the true data,  $\approx 0.045$ , followed by the TPB fit with RMSE  $\approx 0.053$  and

finally the GAM fit with  $\approx 0.14$ . The GAM struggles due to the non-additive (in  $x_1, x_2$ ) nature of the regression function, only being able to model large scale features such as the true function being near to 0 at  $x_1 = \pm 4$ . Adding the “interaction term”  $x_1x_2$  to the GAM model did not improve the fit substantially. Upon visual inspection, MARGARITA and TPB produce similar quality fits in the rectangular region of  $-2 \leq x_1 \leq 2$ . MARGARITA does appear to better reconstruct the features in the boundary region near the corners  $(4, -4), (-4, 4)$ .

## S6 Real Data Analysis

### S6.1 Study Design and Scanning Protocol

All subjects in our study were referred to the University of Rochester Medical Imaging Center and imaged on the same 3T MRI scanner. Study inclusion criteria included history of concussion, while exclusion criteria included dental braces, prior brain surgery, ventricular shunt, skull fractures, or other standard contraindications for MR imaging. Diagnosis of concussion was made by neurologists, physical medicine and rehabilitation physicians, and sports medicine physicians. The control group consisted of young athletes with no history of concussion. The University Institutional Review Board approved this retrospective study. All MRI examinations were reviewed by an experienced neuroradiologist for any artifacts that might affect the quality of the study, as well as for the presence of recent or remote intracranial hemorrhage, signal abnormalities in the brain, hydrocephalus, congenital or developmental anomalies.

The diffusion MRI data was collected on a single 3T scanner using a 20-channel head coil (Siemens Skyra, Erlangen, Germany). Diffusion imaging was performed with a b-value of  $1000 \frac{s}{mm^2}$ , using 64 diffusion-encoding directions. In addition, a  $b = 0 \frac{s}{mm^2}$  image was collected for signal normalization. Additional dMRI parameters included:  $FOV = 256 \times 256mm$ , number of slices = 70, image resolution =  $2 \times 2 \times 2mm^3$ ,  $TR/TE = 9000/88ms$ , Generalized autocalibrating partially parallel acquisition (GRAPPA) factor = 2. Acquisition of dMRI data took 10 minutes and 14 seconds. A Gradient-recalled echo (GRE) sequence was also collected with  $TEs = 4.92, 7.38ms$  at the same resolution of the dMRI to correct

for susceptibility-induced distortion effects.

## **S6.2 Additional Analysis of Data Driven ROI**

Wang et al. (2016) found increased FA in the middle cerebellar peduncle (MCP) is associated with increased cognitive impairment. Xiong et al. (2014) found decreased FA in the superior longitudinal fasciculus (SLF) in patients with TBI. We note that both of these studies were completed in acute cases of TBI, whereas our data represents a more chronic state of TBI (often called post-concussive syndrome). That being said, these tracts are thought to be altered because of the nature of biophysical forces suffered in TBI. In all TBI, there is rotation of the head around the neck, which causes shearing and stretching of the brain stem tracts. In addition, the longer tracts in the brain, including the SLF, are subject to shearing forces on left to right rotation of the head around the neck. In fact, Post et al. (2013) found that mechanical strain in the brain stem and cerebellum are significantly correlated with angular acceleration of the brain, suggesting fibers in this area are susceptible to changes related to TBI. In addition, Brandstack et al. (2013) found changes in long WM tracts in the brain using tractography on subjects with TBI. Therefore, our findings of changes in the MCP and SLF are consistent with the hypothesized mechanism and previous findings in TBI.